SOUTHAMPTON OCEANOGRAPHY CENTRE

RESEARCH & CONSULTANCY REPORT No. 89

Closing the heat budget of the SOC climatology through spatially dependent inverse analysis parameter adjustment

J P Grist and S A Josey

2004

COAPEC Project - Balancing the Atlantic Heat and Freshwater Budgets, Report No. 3

James Rennell Division for Ocean Circulation and Climate
Southampton Oceanography Centre
University of Southampton
Waterfront Campus
European Way
Southampton
Hants SO14 3ZH UK
Tel: +44 (0)23 8059 7738
Fax: +44 (0)23 8059 6400
Email: jyg@soc.soton.ac.uk

DOCUMENT DATA SHEET

AUTHOR
GRIST, J P & JOSEY, S A

PUBLICATION DATE
2004

TITLE
Closing the heat budget of the SOC climatology through spatially dependent inverse analysis parameter adjustment.
(COAPEC Project - Balancing the Atlantic Heat and Freshwater Budgets, Report No. 3)

REFERENCE
Southampton Oceanography Centre Research and Consultancy Report, No. 89, 32pp. & figs.
(Unpublished manuscript)

ABSTRACT

Previous research aimed at closing the heat budget of the Southampton Oceanography Centre (SOC) air-sea flux climatology through the method of inverse analysis is extended to include spatially dependent parameter adjustments and error specification. In earlier analyses, a balanced solution was achieved using globally fixed parameter adjustments, primarily an increase of 19% to the latent heat flux and a reduction of 6% to the shortwave flux. In the new method, the global ocean is divided into various sub-regions in order to allow the parameter adjustments to vary spatially. With this approach a balanced version of the SOC climatology is obtained that requires smaller adjustments, in the range 2-12%, to the latent heat flux than previously but larger changes to the shortwave, up to 18%, depending on region. In addition to enabling direct spatial dependence of the parameter adjustments we have also explored the possibility of making the parameter error spatially dependent both by sub-region and through a dependency on observation density. The various solutions obtained have been evaluated both through the large scale implied ocean heat transport and local comparisons with research buoy measurements. Some improvement is found in the level of agreement of the heat transport with the applied constraints but the buoy comparisons reveal similar problems to those obtained in our previous research. Further, the larger adjustment to the shortwave flux with the new solutions leads to significant differences with respect to satellite based estimates of this component of the flux. We conclude that the earlier solution in which the latent heat flux is increased by 19% is in better agreement with independent estimates than the new spatially dependent solutions. It is thus our preferred means of closing the SOC climatology heat budget imbalance through inverse analysis.

KEYWORDS
air-sea fluxes, COAPEC, inverse analysis, project, ocean heat budget, SOC climatology

ISSUING ORGANISATION
Southampton Oceanography Centre
University of Southampton
Waterfront Campus
European Way
Southampton SO14 3ZH
UK

ABSTRACT

Previous research aimed at closing the heat budget of the Southampton Oceanography Centre (SOC) air-sea flux climatology through the method of inverse analysis is extended to include spatially dependent parameter adjustments and error specification. In earlier analyses, a balanced solution was achieved using globally fixed parameter adjustments, primarily an increase of 19% to the latent heat flux and a reduction of 6% to the shortwave flux. In the new method, the global ocean is divided into various sub-regions in order to allow the parameter adjustments to vary spatially. With this approach a balanced version of the SOC climatology is obtained that requires smaller adjustments, in the range 2-12%, to the latent heat flux than previously but larger changes to the shortwave, up to 18%, depending on region. In addition to enabling direct spatial dependence of the parameter adjustments we have also explored the possibility of making the parameter error spatially dependent both by sub-region and through a dependency on observation density. The various solutions obtained have been evaluated both through the large scale implied ocean heat transport and local comparisons with research buoy measurements. Some improvement is found in the level of agreement of the heat transport with the applied constraints but the buoy comparisons reveal similar problems to those obtained in our previous research. Further, the larger adjustment to the shortwave flux with the new solutions leads to significant differences with respect to satellite based estimates of this component of the flux. We conclude that the earlier solution in which the latent heat flux is increased by 19% is in better agreement with independent estimates than the new spatially dependent solutions. It is thus our preferred means of closing the SOC climatology heat budget imbalance through inverse analysis.

1. INTRODUCTION

This report forms part of a series describing results from a Natural Environment Research Council (NERC) Coupled Ocean-Atmosphere Processes and European Climate (COAPEC) programme funded project. The project has the primary aim of producing a balanced global set of ocean-atmosphere heat exchange fields using the previously developed Southampton Oceanography Centre (SOC) climatology as a basis. It is well recognised that ship-based estimates of air-sea heat fluxes, such as the SOC climatology, have thus far been unable to produce a balanced ocean heat budget. In earlier work carried out within this project (Grist and Josey 2002, 2003; hereafter GJ02 and GJ03) we produced a balanced version of the SOC climatology by using the inverse analysis method of Isemer et al. (1989, hereafter IWH) with spatially fixed parameter adjustments. Here we describe results from an extension of the IWH method to allow for spatially varying parameter adjustments and errors.

In the IWH method, the net heat flux is adjusted by constraining the climatologically implied ocean heat transport to agree with independent hydrographic estimates of the same quantity. By taking advantage of the broad range of ocean heat transport estimates obtained during the World Ocean Circulation Experiment (WOCE) period, we were able in GJ02 and GJ03 to increase the number and spatial distribution of constraints used compared to previous inverse analysis studies. Up to ten estimates throughout the Atlantic and North Pacific were employed as constraints, which compares with a maximum of three in the earlier studies (da Silva et al. 1994; IWH). Various solutions were obtained and these are described in detail in GJ02 and GJ03. The preferred (on the basis of agreement with independent observations) solution required an increase of 19% to the latent heat flux and reduction of 6% to the shortwave flux.

The adjusted SOC fluxes with this solution were found to agree to within 7 Wm^{-2} with large scale area average heat flux estimates obtained using a hydrographic section at 32^{O} S that was withheld from the analysis. Good agreement was also found with other estimates of the global ocean heat transport obtained using residual techniques and atmospheric model reanalysis. However, comparisons with Woods Hole Oceanographic Institute research buoys provided mixed results with improvements at two of the four sites considered and significantly worse agreement at the other two sites. This confirmed the conclusion of Josey et al. (1999) that a global adjustment of the SOC climatology that reduced the shortwave and increased the latent heat would cause the adjusted flux estimates to diverge from the buoy values in certain regions.

In an attempt to resolve the biases with respect to the buoys, we have investigated further developments to the inverse analysis technique. IWH suggested that a suitable way to improve on their method would be to allow the parameter adjustments to vary spatially and seasonally. In this report we present results from an extension of the inverse analysis to allow spatially varying

parameter adjustments. The structure of the report is as follows. In Section 2, the data used in the study is briefly described. The extension of the inverse analysis method to include spatially varying parameter adjustments is then discussed in Section 3. The results obtained with the new analysis method are described in Section 4. Finally, we summarise and discuss the implications of our study in Section 5.

2. PRIMARY DATASET AND CONSTRAINTS

Our analysis is an extension of GJ03 for which the primary dataset employed was the SOC climatology. The SOC climatology is derived from ship reports in the Comprehensive Ocean - Atmosphere Dataset 1a (Woodruff et al., 1993), covering the period 1980-1993. Additional information regarding observing procedure was merged onto this dataset from the International List of Selected, Supplementary and Auxiliary Ships which is published annually by the World Meteorological Organisation (e.g. WMO, 1993). The method used for the production of the climatology is fully described in Josey et al. (1998). Results from an evaluation of the climatology using hydrographic and research buoy measurements are discussed in Josey et al. (1999). For the inverse analysis we have utilized the SOC climatological mean fields of the shortwave, longwave, latent and sensible heat fluxes.

The constraints on the inverse analysis employed for the present study comprise various hydrographic estimates of the ocean heat transport together with the requirement of global heat budget closure to within ± 2 Wm^{-2}. The latter is expressed as zero net heat transport across the boundary of the Southern Ocean with Antarctica with an error bar of 0.65 PW. The different heat transport estimates together with the source of each are listed in Table 1; each estimate has been given a constraint number for ease of reference. Note that an error estimate has been listed for each of the heat transport values used as constraints. These error estimates have been taken from the source reference relevant to each section. We note that the constraints used are the same as in GJ03 and GJ02, with the exception that we have now use an updated value for the A11 South Atlantic section of 0.43 ± 0.08 PW (McDonagh and King, 2004).

In addition to the hydrographic measurements listed in Table 1, a more recent estimate of ocean heat transport for the Indian/Pacific basin across 32^{O} S (Wijffels et. al, 2001) is used to evaluate the results. Further evaluation is provided by comparison with residual method values obtained from the NCEP/NCAR atmospheric model reanalysis (Trenberth and Caron, 2001) and with independent measurements of surface fluxes from various research buoys (Weller et al., 1995; Weller and Anderson, 1996; Moyer and Weller, 1997; Weller et al., 1998). Further details of the buoy deployments are provided in Josey et al. (1998).

3. THE INVERSE METHOD

In this section, we present details of the extension to the inverse method used previously in GJ02 and GJ03. Our aim is to balance the SOC climatology using a revised version of the method which allows for spatially varying rather than fixed parameter adjustments. In order to do this, we divide the ocean into sub-regions each of which has a different set of parameter adjustments for the four components (latent, sensible, longwave, shortwave) of the net heat flux. There are a wide variety of ways in which these regions could be defined and we have focused primarily on solutions in which the sub-regions are latitudinal bands. However, in addition we have also considered sub-regions which are defined by the number of ship observations and therefore have an irregular spatial distribution as detailed later (Sec 3.2.3).

3.1. Formulation of Method

First, we review the key elements of the inverse analysis method and describe its extension to include spatially dependent parameter adjustments. Previously we have noted (GJ03 equation 3) that the unadjusted heat transport across a given constraint latitude $\phi_{(j)}$ may be written:

$$H^*_{\phi(j)} = H_0 - \int_{\phi_0}^{\phi_{(j)}} \int_{\lambda_{1(j)}}^{\lambda_{2(j)}} Q^*_N(\phi,\lambda,p^*_1,...,p^*_m)\,d\lambda\,d\phi \qquad (1)$$

where H_0 is the ocean heat transport at some northern reference latitude, ϕ_0, (note we use the same northern reference values as in GJ03, see Table 1) ; Q^*_N is the net heat flux, and $p^*_1,...,p^*_m$ are i = 1, m adjustable parameters. The longitudes $\lambda_{1(j)}$ and $\lambda_{2(j)}$ refer to the western and eastern limits (respectively) of the ocean basin at a given latitude. For our original analysis we defined four adjustable parameters, $(p^*_E,p^*_H,p^*_S,p^*_L)$ which were coefficients on the latent heat, Q^*_E , sensible heat, Q^*_H, shortwave, Q^*_S, and longwave, Q^*_L, flux estimates. With these free parameters, (1) can be written:

$$H^*_{\phi(j)} = H_0 - \int_{\phi_0}^{\phi_{(j)}} \int_{\lambda_{1(j)}}^{\lambda_{2(j)}} (p^*_E Q^*_E(\phi,\lambda) + p^*_H Q^*_H(\phi,\lambda) + p^*_S Q^*_S(\phi,\lambda) + p^*_L Q^*_L(\phi,\lambda))\,d\lambda\,d\phi \qquad (2)$$

In contrast to our previous analysis, we now divide the global ocean into k = 1, r latitude bands and define ϕ_{k-1} and ϕ_k to be the northern and southern limits of band k (see example case in Fig. 1a and note that neighbouring bands share a common boundary). We allow the free parameters to vary in value between each latitude band, as well as each flux component, so we now have a total of m = 4*r parameters. Individual parameters are designated by a flux component and a latitude band index, e.g. p^*_{E1} is the latent heat flux parameter for band 1. The m free parameters are then $(p^*_{E1},p^*_{H1},p^*_{S1},p^*_{L1},...,p^*_{Er},p^*_{Hr},p^*_{Sr},p^*_{Lr})$ and we can write,

$$H^*_{\phi(j)} = H_0 \left[\begin{array}{l} \int_{\phi_1}^{\phi_0} \int_{\lambda_1(j)}^{\lambda_2(j)} (p^*_{E1} Q^*_E(\phi,\lambda) + p^*_{H1} Q^*_H(\phi,\lambda) + p^*_{S1} Q^*_S(\phi,\lambda) + p^*_{L1} Q^*_L(\phi,\lambda)) d\lambda d\phi + \\ \int_{\phi_2}^{\phi_1} \int_{\lambda_1(j)}^{\lambda_2(j)} (p^*_{E2} Q^*_E(\phi,\lambda) + p^*_{H2} Q^*_H(\phi,\lambda) + p^*_{S2} Q^*_S(\phi,\lambda) + p^*_{L2} Q^*_L(\phi,\lambda)) d\lambda d\phi + \\ \ldots + \\ \int_{\phi(j)}^{\phi_{k(j)-1}} \int_{\lambda_1(j)}^{\lambda_2(j)} (p^*_{Ek(j)} Q^*_E(\phi,\lambda) + p^*_{Hk(j)} Q^*_H(\phi,\lambda) + p^*_{Sk(j)} Q^*_S(\phi,\lambda) + p^*_{Lk(j)} Q^*_L(\phi,\lambda)) d\lambda d\phi \end{array} \right] \quad (3)$$

where k(j) is the index of the latitude band that has it's northern boundary immediately to the north of the latitude $\phi_{(j)}$.

The solution to the inverse analysis is obtained by minimising the difference between heat transport estimates at various latitudes inferred from the adjusted field and corresponding constraint values from hydrographic section measurements, subject to the further constraint that a weighted sum of the parameter adjustments should be as small as possible (see GJ03 for details). We designate by, $\hat{H}_{\phi(j)}$, the hydrographic estimates of the heat transport, at the constraint latitudes $\phi_{(j)}$ where j = 1, n. The adjustments to each parameter may then be obtained in the same way as in GJ03, the solution vector of the parameter adjustments being,

$$\mathbf{x} = \mathbf{W}_e^{-1} \mathbf{A}^T \left[\mathbf{A} \mathbf{W}_e^{-1} \mathbf{A}^T + \mathbf{W}_\phi^{-1} \right]^{-1} \mathbf{h} \qquad (4)$$

As in GJ03, $\mathbf{W}_e$ = diag(e_{E1}^{-2},...,e_{Lr}^{-2}) is a square matrix containing the reciprocals of the parameter errors squared on the diagonal, $\mathbf{W}_\phi$ = diag(ϕ_1^{-2},..., ϕ_n^{-2}) is the weighting matrix of the square of the constraint errors and **h** is a vector of dimension n containing the difference ($\hat{H}_{\phi(j)}$ - $H^*_{\phi(j)}$) between the constraint's heat transport value and the original estimate for each of the n constraints. The n by m matrix **A** contains the sensitivity terms, that is the elements given by,

$$A_{ji} = \partial H^*_{\phi(j)} / \partial p^*_i \qquad (5)$$

thus, the sensitivity terms are the partial derivatives of the heat transport at each constraint latitude with respect to each of the m=4*r parameters; the index i thus runs from i=1,4r. For example, for the term associated with the first constraint and parameter p_{E1}, we find,

$$A_{1\,1} = \partial H^*_{\phi(1)} / \partial p^*_{E1} = \int_{\phi_1}^{\phi_0} \int_{\lambda_1}^{\lambda_2} \partial Q^*_N(\phi,\lambda) / \partial p^*_{E1} \, d\lambda d\phi \qquad (6a)$$

$$= \int_{\phi_1}^{\phi_0} \int_{\lambda_1}^{\lambda_2} Q^*_E(\phi,\lambda) \, d\lambda d\phi \qquad (6b)$$

The other terms may be obtained in a similar manner, as shown in the following example elements of the sensitivity matrix. For the second constraint and first parameter (p_{E1}),

$$A_{21} = \int_{\phi_2}^{\phi_1} \int_{\lambda_1}^{\lambda_2} Q^*_E(\phi,\lambda)\, d\lambda\, d\phi \qquad (7a)$$

while, for the second constraint and sixth parameter (p_{H2}),

$$A_{26} = \int_{\phi_2}^{\phi_1} \int_{\lambda_1}^{\lambda_2} Q^*_H(\phi,\lambda) d\lambda\, d\phi, \qquad (7b)$$

Note that if a constraint j is at a latitude $\phi_{(j)}$ north of the northern edge of latitude band k (that is ϕ_{k-1},), then, $H^*_{\phi(j)}$ (Equation 3) will have no dependency on any parameter with a band index greater than k-1. Thus, the **A** matrix will contain a significant proportion of zero elements.

3.2 Specification of the Sub-Regions and Parameter Error

In addition to defining separate parameters for each sub-region it is also necessary to specify the error on each parameter ($e_{E1},...,e_{Lr}$). We have explored three different formulations of the sub-regions and parameter errors. Details of these three formulations are given in this section.

3.2.1 Formulation 1: Latitude Band Dependent Parameters with Spatially Fixed Errors

In this formulation (F1), the values of the parameter adjustments are allowed to vary between sub-regions as detailed above, but the parameter error is defined to be spatially constant and equal to 0.2 for all parameters as in GJ03. The constraint of a balanced heat budget to within ± 2 Wm^{-2} (as in GJ03 Solution 3) and all 10 hydrographic constraints were used so that the total number of constraints, n = 11. As regards the sub-regions, these were defined to be latitude bands which were selected in such a way that the bands had approximately equal area. For this formulation we have adopted the same number (11) of bands as there are constraints, see Fig. 1. A more complex, observation frequency dependent definition of the sub-regions is explored in Formulation 3 detailed below. With the sub-regions and parameters as defined, **A** is an n (= 11) x m (= 44) matrix; $\mathbf{W_e}$ is a 44 x 44 diagonal matrix with values equal to 0.04; $\mathbf{W_\phi}$ is an 11 x 11 matrix and **h** is a 1 x 11 vector. $\mathbf{W_\phi}$ and **h** remain the same as in GJ03 Solution 3, with the exception that the updated estimate for constraint 7 is now used.

3.2.2 Formulation 2: Latitude Band Dependent Parameters with Spatially Varying Errors

In F1 we assumed that the error associated with the fluxes is spatially fixed at 0.2 for each of the flux components. This assumption is refined in Formulation 2 (F2) to allow variation in the parameter error between boxes. It is reasonable to expect the errors in the flux estimates to

increase as the number of observations decreases (e.g. Legler, 1991). In addition, the number of observations per grid box may as a first approximation be considered a simple function of latitude as the sampling frequency falls away sharply at lower latitudes (e.g. Josey et al., 1999). Thus, we repeated the analysis of F1 with the two different estimates of the parameter error shown in Fig. 2 which are intended to qualitatively reflect the density of observations in the SOC climatology. In the first case (F2a) the estimated parameter error, which is assumed to be the same for all 4 parameters in a given sub-region, increases from 0.2 in the well-sampled Northern Hemisphere to 0.3 in the poorly-sampled Southern Hemisphere. In the second case (F2b) the parameter error increases more rapidly from 0.1 in the Northern Hemisphere to 0.3 in the Southern Hemisphere. Also shown in Fig. 2, for qualitative comparison, is the latitudinal variation of $(1/\sigma)$, where σ is the square root of the zonally averaged observation density per one-degree grid cell for an example month January 1986.

3.2.3 Formulation 3: Observation Density Dependent Parameters and Errors

The formulations of the inverse method described above (F1 and F2) involved dividing the global ocean into 11 latitudinal bands. It is, of course, also possible to divide the ocean in many other ways. A more general form of (3), in which we define k = 1, r distinct regions is given by,

$$H^*_{(j)} = H_0 - \int_{\alpha(j)}^{\alpha_0} \int_{\lambda(j)}^{\lambda_2(j)} \sum_{k=1,r} \sum_{a=1,A} \sum_{b=1,B} \Delta_{kab}(p^*_{Ek}Q^*_{E\,a,b} + p^*_{Hk}Q^*_{H\,a,b} + p^*_{Sk}Q^*_{S\,a,b} + p^*_{Lk}Q^*_{L\,a,b})dS_{a,b} \quad (8)$$

where there are a = 1, A longitudinal elements and b = 1, B latitudinal elements in the data set; $Q^*_{Ea,b}$ represents the mean latent heat flux from the grid cell defined by index pair (a,b) (and likewise for the other heat flux components); Δ_{kab}, is defined to equal 1 if (a,b) is in region k and 0 if not, and $dS_{a,b}$ is the area of the grid cell (a,b). For the case of the SOC climatology the longitudinal and latitudinal elements are the edges of the cells which form the global 1^o x 1^o grid.

In this general form, we can define the spatial extent of the different regions in a more complex manner than previously. In particular we have explored the case where the regions are determined by the number of observations. The spatial distribution of the density of the observations in the SOC climatology for January 1986 is shown in Fig. 3. Note that this field has been interpolated from the original raw mean 1^o x 1^o observation density fields using the same objective analysis procedure employed to produce the SOC climatology flux fields (Josey et al., 1999). In Formulation 3 (F3) we define the k = 11 regions in a way that reflects the spatial distribution of the density of the SOC climatology observations using the values from this example month. Region 1 is defined to have the highest density of observations and region 11 the lowest density, details of the regions are given in Fig. 4. The regions have been defined such that, as in F1 and F2, they have similar areas see Fig. 5. Note that we will consider several variants of F3 which have different prescribed parameter errors, these will be detailed in Sec. 4.1.3.

4. RESULTS

In this section, we summarise the principal results obtained from the various formulations of the spatially dependent inverse analysis problem, detailed above, when applied to the SOC climatology. We also include an evaluation of the different solutions in terms of the implied ocean heat transport and comparisons with measurements made by research buoys at key locations.

4.1 The Inverse Analysis Solutions

4.1.1 Formulation 1

We begin with Formulation 1 (F1) in which the adjustable parameter error is globally fixed at a value of 0.2 for all components but the parameters themselves are allowed to take different values in each of the 11 latitude bands defined in Fig.1a. The values of the parameter adjustments for the inverse analysis solution in this case are shown in Fig. 6 (solid lines) and listed in Table 2. Also shown on the right hand axis of the figure are the globally fixed adjustments from Solution 3 of GJ03. The parameter adjustments for latent heat, sensible heat and longwave are smaller for F1 than for Solution 3 across all latitude bands. In particular, the latent heat flux adjustments are now in the range 2-13% compared with 19% for Solution 3. In contrast, the shortwave parameter adjustments are typically larger (up to 17%) for F1 than for Solution 3 (6%). Thus the primary effect of introducing a spatial dependence of the parameter adjustment has been to shift the major change in the heat flux from the latent to the shortwave component. This is readily apparent if one compares area weighted values of the F1 parameter adjustments with the spatially fixed GJ03 Solution 3 (last two rows of Table 2). The mean latent heat adjustment deceases from 19% to 7% while the shortwave adjustment doubles from 6% to 12%. There are also smaller adjustments in the mean to the longwave and sensible heat parameters.

As discussed in GJ03, IWH suggested an acceptability criterion for inverse analysis solutions that the magnitude of each adjustment should be less than the prescribed parameter error, which in this case is 20%. Thus, the F1 solution meets the IWH criterion for all the components and all latitude bands. However, whereas in GJ03 the global adjustment to latent heat (19%) was close to the maximum allowed, in F1 the adjustments are more moderate and there are only two bands, in which one of the components (shortwave) requires greater than 15% adjustment. For all the F1 parameters, the adjustments are greatest in the Northern Hemisphere (in particular in bands 1 and 2) and they decrease steadily towards the Tropics and the Southern Hemisphere. Note this is not an artifact of choosing a northern reference latitude for the inverse analysis and integrating the heat transport southwards as we have obtained very similar solutions (not detailed here) when a southern reference latitude and northward integration have been employed.

Global fields of the inverse analysis adjustment for each component of the heat flux and the net heat exchange are shown in Fig. 7; also shown is the resulting adjusted net heat flux field.

Unsurprisingly, the fields exhibit discontinuities in some case between adjacent bands because we have not attempted to impose a requirement at this stage that the adjustments in neighbouring bands be of similar magnitudes. Smoothed versions of the fields will be discussed below but first we consider the global means of the unsmoothed adjustments for F1 which are compared with those for Solution 3 GJ03 in Table 3. As expected, from the discussion of the parameter adjustment values above, F1 makes a smaller adjustment to the latent heat, sensible heat and longwave, and an increased adjustment to the shortwave compared to GJ03 Solution 3. The most important changes are to latent heat, which formerly accounted for -17 Wm^{-2} but now only accounts for -6 Wm^{-2} and the shortwave adjustment which has increased in size from -10 Wm^{-2} in Solution 3 to -22 Wm^{-2} with F1.

Like GJ03 Solution 3, the F1 adjusted net heat flux field is very close (less than 1 Wm^{-2} for F1 and within 2 Wm^{-2} for Solution 3) to global balance. However, there are significant regional differences in the net heat fluxes of the 2 solutions. The area averaged net heat adjustments, for the different solutions, for each of the latitude bands are shown in Fig. 8 and in Table 4. The new solution F1 requires greater adjustments to the net heat flux than Solution 3 GJ03 in the Northern Hemisphere (for example -45 Wm^{-2} in Band 2 compared with –36 Wm^{-2} for the same band in Solution 3) but smaller adjustments in most of the Tropics and the Southern Hemisphere. This difference reflects the ability of the spatially dependent inverse analysis formulation to produce greater adjustments in regions where the discrepancy between hydrography and the SOC climatology is greater (in particular the k = 2 band which contains the western boundary current regions in the North Atlantic and North Pacific Oceans).

As noted above, no constraint has been applied to force the adjustments in neighbouring boxes to be similar and as a consequence there are discontinuities in the adjusted fields. A smoothed version of the adjusted fields has been obtained by interpolating the points on Fig. 6 to match the latitudinal resolution of the SOC climatology. We used a polynomial (cubic) interpolation between bands 1 and 11. For the latitudes north of the mid-point of band 1 we fix the adjustment to be equal to the mid-point of band 1. Likewise for the latitudes south of the mid-point of band 11 we fix the adjustment to be equal to the mid-point of band 11.

Comparison of the interpolated and unsmoothed solutions for F1 (Fig. 6) shows that the interpolated parameter adjustments remain very close to the original values. The adjustment fields and the adjusted net heat flux field resulting from the smoothed F1 solution are shown in Fig. 9. The main features of the smoothed adjusted fields remain the same as in the unsmoothed version and the net heat fluxes within each latitude band are very similar in each case (Fig. 8 and Table 4). The values listed in Table 4 show that the difference is 1 Wm^{-2} or less for 7 latitude bands and 2 Wm^{-2} for the other 4 latitude bands. Hereafter, when referring to the F1 solution, and F2 detailed below, we will be referring to the smoothed solutions. The difference between the net heat flux of GJ03 Solution 3 and the smoothed F1 field is shown in Fig. 10a. In addition, the zonally averaged net heat flux adjustment for Solution 3 and F1 are plotted on Fig. 10b. These figures clearly show

that the heat flux adjustment is more strongly concentrated in the Northern Hemisphere when the spatially dependent F1 formulation of the inverse analysis is employed.

In the F1 results presented above a fixed number (11) of latitude bands were specified. We have also explored the impact on the solution of varying the number of latitude bands. The results of these additional analyses are briefly summarised here using solutions obtained for two cases (6 and 16 latitude bands) in which the number of regions is first less and then greater than the F1a formulation. Note that the other aspects of the inverse analysis are as before and that in each case the bands have been chosen such that they are all of approximately equal area. The solutions for the 6, 11 and 16 band cases are compared in Fig. 11. The parameter adjustments are broadly similar in magnitude in each case with a trend towards larger adjustments in the Northern Hemisphere. The level of variability about this trend increases slightly with the number of latitude bands but the trend itself and the relative magnitude of the adjustments for the four components is not noticeably different for the range of band numbers considered. Thus, the main characteristics of the solution do not appear to be strongly dependent on the number of bands specified within the range that we have investigated.

4.1.2 Formulation 2

We now consider the extension of F1 to the case in which the specified parameter error is allowed to vary with latitude rather than being held constant. The inverse analysis solution for Formulation 2a in which the parameter errors increase with decreasing latitude from 0.2 to 0.3 is shown in Fig. 12; the corresponding adjusted fields are in Fig. 13. In order to determine the impact of using spatially varying parameter errors, the solution for F1 is also shown in Fig. 12. The impact is small and only noticeable in the Southern Hemisphere which is to be expected given that the Northern Hemisphere errors are close to those adopted for the F1 case. Between 10^{O} S and 30^{O} S, the adjustments to latent heat, longwave and shortwave are slightly smaller in F2a than F1. South of 30^{O} S, the reverse is true with F2a requiring slightly larger adjustments to these components than F1. There is negligible difference in the adjustment to the sensible heat flux. The difference in area-averaged net heat flux by latitude band from the original SOC climatology for each band is given in Table 4 and Figure 8. There are no bands in the Northern Hemisphere where the F2a and F1 adjustments differ by greater than 1 Wm^{-2}. In the Southern Hemisphere, in Band 7 (10^{O} S - 20^{O} S) the adjustment is smaller in F2a than F1 by 2 Wm^{-2}, whereas in Bands 9 and 10 (30^{O} S - 50^{O} S), F2a makes a larger adjustment by 3-4 Wm^{-2}. Thus, in general the F2a solution differs by no more than 4 Wm^{-2} from F1 in the size of the adjustments to the original SOC net heat flux. When one considers the global mean adjustments to the flux components (Table 3) there is no difference between F1 and F2a.

We have also investigated a modified version of F2a, referred to as F2b, in which the errors are reduced towards a lower limit of 0.1 in the highest latitude Northern Hemisphere band. The parameter adjustments for the F2b solution are compared with F2a in Fig. 14. The two

solutions are broadly similar, the most notable difference being that F2b has smaller adjustments than F2a north of 40^{O} N and south of 40^{O} S. At most other latitudes F2b has very similar adjustments to F2a. If the adjustments are considered in terms of their global averages then it is clear the two solutions result in almost identical changes to the components of the heat flux (Table 3). However, when one considers the validity of solution F2b, the IWH criterion (that the parameter adjustment must be less than the specified error) is not met for shortwave in bands 1, 2 and 3, so the solution is not acceptable on these grounds.

In summary, allowing the prescribed parameter error to vary in the manner of solutions F2a and F2b has not led to major changes in the resulting parameter adjustments relative to the F1 solution in which the parameter error was fixed. This suggests that the prescribed parameter error is of secondary importance to the magnitude of the discrepancy between the climatology and hydrography in determining the nature of the solution.

4.1.3 Formulation 3

Having explored solutions obtained with a simple latitudinal dependence of the parameter adjustments we now consider results obtained with the F3 formulation in which the spatial dependence is defined in terms of observation density as described earlier. The solutions for F3 are displayed in Fig. 15 in a similar manner to the results of F1 and F2. The numbers on the x-axis now represent regions with a given observation frequency, as defined in Fig. 4, rather than latitude bands. The lower numbers tend to be associated with the more northerly latitudes and the higher numbers with the more southerly ones because the low numbers represent high observation frequency regions which are mainly in the Northern Hemisphere.

We present solutions to three variations on the F3 formulation. In the first solution (F3a) the parameter error is spatially fixed at 0.2 while in the second (F3b) it increases from 0.1 to 0.3 as the observation density decreases. Considering these two solutions first, the parameter adjustments are broadly similar in each case. There are some minor differences, specifically the F3b solution has smaller adjustments in the highest observation frequency, lowest error Region 1. In this region the shortwave adjustment reduces from -0.21 to -0.16 and the latent heat adjustment reduces from 0.13 to 0.11. This is compensated by F3b having a greater adjustment in the regions of intermediate observation density (Regions 5, 6 and 7). However, both of these solutions marginally fails to meet the IWH acceptability criterion as the shortwave adjustment exceeds the estimated error in the region with the highest observation density.

By experimenting with various definitions of the parameter error, we have found that to obtain a solution which is acceptable it is necessary to increase the assumed parameter errors to 0.26 in areas 1 to 4 and we refer to this case as our third solution (F3c). This solution and the associated adjustments are shown in Fig. 15c and Fig. 16 respectively. The adjustments are similar to F3a and F3b although now within the prescribed error limits. Note that there are abrupt

discontinuities in the adjustments to the fluxes between different areas as there is no constraint that adjustments in adjacent regions should be similar and we have not interpolated the resulting fields. The adjusted fields produce a heat budget that is close to balanced, i.e. the global mean adjusted net heat flux is 0.4 Wm^{-2}, and the adjustments to the individual components (Table 3) are again very similar to F1 and F2.

To summarise, we have obtained a range of solutions (F1, F2a and F3c) using plausible definitions for the parameter adjustments and errors which satisfy the IWH criterion. These solutions tend to require smaller adjustments to the latent heat and larger ones to the shortwave than was the case with GJO3 Solution 3 in which the parameter adjustments and errors were spatially fixed. In addition, in all cases the global mean adjusted net heat flux is less than 1 Wm^{-2}. This value represents a small net oceanic heat gain rather than the slight heat loss of GJ03 Solution 3 for which the global mean was –2 Wm^{-2}. It is not as yet clear whether the new solutions represent an advance on GJ03 Solution 3. In the following sections we address this issue by means of comparisons with independent heat transport estimates and buoy measurements.

4.2 Evaluation of the Adjusted Flux Fields

We now evaluate the adjusted flux fields for each of the three new formulations using a variety of measures at spatial scales which vary from global to local. Our aim is to determine whether any of the new solutions can be considered to be an improvement on GJ03 Solution 3.

4.2.1 Comparisons with Regionally Implied Heat Fluxes from Hydrography

Area averaged net heat fluxes obtained from the original SOC climatology, GJ03 Solution 3 and the new formulations F1a, F2a and F3c are compared with those implied by hydrography in Fig. 16. A similar comparison was carried out in GJ03 and our aim here is to determine whether the new formulations bring the fluxes into closer agreement with hydrography than the earlier Solution 3 in which the parameter adjustments were spatially fixed. Note that the area-averaged fluxes have been derived from the constraints used in the analysis (Table 1) with the exception of the new estimate from Wijffels et al. (2001) at 32° S, indicated by the dashed line. The comparison is thus intended to be primarily a test for consistency of the adjusted fluxes with the applied constraints.

The results of the comparison are broadly similar to those found in GJ03. For the 12 regions considered, the mean magnitude of the difference between the adjusted fluxes and hydrography is 9 Wm^{-2} for GJ03, 8 Wm^{-2} for F1a and 8 Wm^{-2} for F2a. Thus, the two formulations with latitudinally varying parameter adjustments have not significantly improved the agreement with hydrography. Moreover, they now generate a higher value for the most extreme difference, which is 24-25 Wm^{-2} in the most northern region of the Pacific, compared to 18 Wm^{-2} with

Solution 3. Similar results are obtained with solution F3c, in which the parameter adjustments depend on the number of observations, the difference with respect to hydrography being 9 Wm^{-2}.

Considering the regions adjacent to the 32° S line, encouraging agreement (to within 10Wm^{-2}) is again obtained with the various new solutions compared to the biases of 17 and 41 Wm^{-2} with the original SOC climatology. Thus, overall, the new formulations maintain the improvements found with GJ03 Solution 3 relative to the original SOC fields but do not lead to any significant improvements. In the next section, we investigate whether this remains the case when the implied ocean heat transport is considered.

4.2.2 Climatologically Implied Ocean Heat Transport

The climatologically implied ocean heat transports for F1, F2a and F3c, in the Atlantic, Pacific and Global Ocean basins are shown in Fig. 18. For reference, the hydrographic constraints used in the analysis and heat transport estimates from GJ03 Solution 3 and Trenberth's residual analysis of the NCEP/NCAR atmospheric reanalysis (Trenberth and Caron, 2001) are included on the figure. Also shown (red cross with error bars) is an estimate of the global ocean heat transport at 30° S which was determined (see GJ03) using recent hydrographic measurements of the transport across these latitudes in the Indian and Pacific Ocean basins that were not employed as constraints on the analysis.

We first consider the F1 and F2a implied transports which are very similar, to the extent that their respective curves overlie each other through much of the latitude range considered, the only exception being the Southern Hemisphere half of the Global Ocean figure, in which case they still agree to within 0.1 - 0.2 PW. The close agreement reflects our earlier finding (Section 4.1.2) that allowing the prescribed parameter error to varying latitudinally (F2a) had little effect on the solution relative to the fixed parameter error case (F1). Note that the F2b solution also results in a very similar implied heat transport to F2a and is not shown. There are, however, significant differences between the F1/F2a estimates and the GJ03 Solution 3 estimate. Specifically, the new method leads to a greater northward heat transport in the Northern Hemisphere which is in better agreement with both the independent Trenberth residual fields and with the hydrographic constraints imposed on the analysis. At the maximum of northward heat transport, around 20° N, the F1/F2a transport is about 0.5 PW greater than GJ03 Solution 3 (by roughly 0.3 PW in the Pacific and 0.2 PW in the Atlantic).

The F1/F2a estimates are, like GJ03 Solution 3, in good agreement with the global hydrographic transport value at 30° S (see panel c.). At the southern boundary of the Global Ocean, the heat transport should go to zero if global closure has been achieved. The new solutions F1/F2a are close to achieving this goal with residual transports of order -0.3 PW which corresponds to the global mean net heat flux of 1 Wm^{-2} noted earlier. By comparison, Solution 3 has an excess northward transport of 0.6 PW which reflects the global mean net heat flux of −2

Wm^{-2} with this solution. Although, the difference in global means is marginal, the improved agreement with the Northern Hemisphere constraints provides some ground for preferring the spatially dependent solutions (F1/F2a) over the previous GJ03 Solution 3 in which the parameter adjustments and errors were spatially fixed.

For Formulation 3, we focus on case F3c as F3a and F3b were unable to satisfy the IWH criterion. The F3c heat transport falls between the values for GJ03 and F1/F2a in the North Pacific and is slightly higher than them in the North Atlantic. In the Southern Hemisphere, the F3c global southward heat transport is about 0.5 PW stronger than the F1/F2a values over much of the latitude range considered. At 30^{o} S it significantly overestimates the magnitude of the transport provided by hydrography and on this basis we are led to prefer the F1/F2a solutions which were both within the error range on the hydrographic value.

In summary, the heat flux fields from F1/F2a (but not F3c) provide estimates of the ocean heat transports which are in good agreement with all of the available constraints and independent measures. They are also in noticeably better agreement with the North Atlantic constraints than was found to be the case with GJ03 Solution 3.

4.2.3 Comparisons with Research Buoys

Having evaluated the fluxes obtained with the new formulations in terms of regionally averaged values and the large scale implied ocean heat transport, we now consider how they compare at a local scale with high quality measurements made by Woods Hole Oceanographic Institution (WHOI) research buoys. Details of these buoys and the comparison technique are given in GJ03. The adjusted fluxes at the location of each buoy are compared with the buoy measurements for the period of each deployment in Table 5a-d and Fig. 19. The figure shows the amounts by which the original SOC climatology, GJ03 Solution 3 and the various new versions (F1, F2a, F3c) of the adjusted fluxes differ from the research buoys. The F1 and F2a fluxes are very similar at the location of the buoys (as are the F2b fluxes not detailed here) so we discuss them together. Considering the flux components first, the smaller latent heat adjustment improves the level of agreement between F1/F2a and the buoys (within 15 Wm^{-2}) relative to GJO3 Solution 3 (26-28 Wm^{-2}) at the Subduction array and TOGA-COARE sites although the agreement is not as good as with the original SOC climatology (within 7 Wm^{-2}). The converse is true for the FASINEX array where the F1/F2a agreement (32-33 Wm^{-2}) is not as good as it is with Solution 3 (21 Wm^{-2}) although better than the original fields (45 Wm^{-2}). At the Arabian Sea site the F1/F2a latent heat fluxes are in closer agreement (within 4 Wm^{-2}) with the buoys than either the original fields (11 Wm^{-2}) or Solution 3 (10 Wm^{-2}).

Although there is some improvement to the latent heat flux, the much larger adjustment to the shortwave in F1/F2a than Solution 3 significantly worsens the level of agreement at 3 of the 4 buoy deployments considered from of order 20 Wm^{-2} with Solution 3 to about 40 Wm^{-2} with the

new fields. The exception to this is the TOGA-COARE site where improved agreement to within 5 Wm^{-2} is obtained. For the other two components, first the sensible heat flux shows only small differences from the buoys with the exception of the FASINEX site where there is a persistent bias of about 7 Wm^{-2} in all of the cases considered. Second, the adjustments to the longwave flux are also relatively small in each case and the level of agreement with the buoys is typically in the range 4-8 Wm^{-2} with GJ03 Solution 3 generally being closest to the buoy values. The F3c component fluxes tend to show a similar pattern of differences from the buoys as F1/F2a, the main difference being in the shortwave flux where much better agreement is obtained at the Arabian sea site and poorer agreement at the FASINEX array.

We now consider the impact that the adjustments have on the net heat flux at the various buoy sites. At the Subduction buoy site the poor level of agreement found with Solution 3 (45 Wm^{-2} difference) has become worse with F1/F2a (53 - 55 Wm^{-2}) and is about the same with F3c (44 Wm^{-2}). For the Arabian Sea and TOGA-COARE buoys, F1/F2a are again marginally worse than Solution 3 while F3c has the best agreement (3-4 Wm^{-2}) of all of the flux fields considered, including the original SOC climatology. At the FASINEX site, F1/F2a now show agreement to within 1 Wm^{-2} with the buoy 'net heat flux' (note longwave is omitted as it was not measured by the buoy), although this is largely due to a fortuitous calculation between differences in the latent and shortwave flux components, while F3c differs by nearly 20 Wm^{-2}.

In summary, the results of the buoy comparisons are disappointing in that the large discrepancies with respect to the Subduction array found with Solution 3 remain with the new spatially dependent adjustments to the flux fields. Better agreement is typically found between the buoy and new latent heat flux estimates but this has been at the expense of much larger differences in the shortwave fluxes, as is to be expected given the shift in the size of the adjustments in these two terms with the spatially dependent formulations. Given the results of the ocean heat transport calculations discussed in Sec. 4.2.2, it could be argued that the F1/F2a formulations represent some improvement on the old Solution 3 but this is not continued in the buoy comparisons. Thus it cannot be said that the inclusion of a spatial dependence in the parameter adjustments has led to a clear improvement in the fields relative to those obtained previously by GJ03 with spatially fixed adjustments.

5. SUMMARY AND DISCUSSION

The overall goal of the research presented here, and in earlier publications (GJ02, GJ03) from the COAPEC funded project, has been to use the method of inverse analysis to resolve the global bias of 30 Wm^{-2} in the original SOC heat flux climatology. In the analyses reported in GJ02 and GJ03 we used globally fixed parameter adjustments for the inverse analysis and obtained a preferred solution in which the global ocean heat budget was closed at the 2 Wm^{-2} level

of uncertainty. This closure was achieved primarily through an increase of 19% to the latent heat flux and a reduction of 6% to the shortwave flux. Here we have presented results from an extension of the inverse analysis to include spatially dependent parameter adjustments and error specification. In the extended method, the global ocean is divided into various sub-regions in order to allow the parameter adjustments to vary spatially.

In our first formulation (F1) of the method, we subdivided the global ocean into 11 approximately equal sub-regions. Each heat flux component was assigned a unique parameter adjustment for each area and the parameter errors were globally fixed. Thus, this formulation represents a simple extension of GJ03 Solution 3 to the case where the parameter adjustments, but not the errors, are spatially dependent. The solution in this case required smaller adjustments (in the range 2 - 12%) to the latent heat flux than observed in GJ03 but larger changes to the shortwave, up to 18%, depending on region. When expressed as area weighted global means, the latent heat adjustment is +7% and the shortwave adjustment –12%. The reduction in the latent heat flux adjustment from 19% to 7% now places it comfortably within the prescribed error range of 20%. However, as noted in GJ03, the adjustment of 19% for the earlier Solution 3 is not unreasonable given the possibility of errors of order 10% in each of the 3 key variables (wind speed, sea-air humidity difference and the transfer coefficient) that drive the latent heat flux. The increase in magnitude of the shortwave adjustment from 6% with Solution 3 to 12% with the new formulations also appears reasonable. However, as discussed in detail below it has the consequence that the global mean shortwave flux is now significantly smaller than recent satellite based estimates.

As an extension of F1 we allowed the prescribed parameter errors to vary with latitude (F2) with the error increasing as the latitude decreased to qualitatively reflect the change in the sampling frequency of the observations. However, the impact on the parameter adjustments of allowing the parameter errors to vary in this way, and the resulting change in the net heat flux, was found to be small. This implied that, for the formulation of the spatial dependence in the inverse analysis considered here, variations in the prescribed parameter error are of secondary importance to the magnitude of the discrepancy between the climatology and hydrography in determining the adjustments.

A further formulation of the method, in which the ocean sub-regions for the different parameters were defined by the number of observations in each grid cell (F3) was also explored. In this case, the parameter errors defined for each of the areas reflected the different observation densities with larger errors in the more poorly sampled areas. Our intention here was to explore the possibility that larger adjustments will be produced if the parameter error in the poorly sampled regions is increased. However, the solution in this case was found to require large adjustments in the well sampled Northern Hemisphere mid-latitude regions rather than the anticipated large changes in poorly sampled regions. This again implies that it is the discrepancy between climatology and hydrography which dominates, within the reasonable range of

parameter error definitions that we have employed, as it is in the Northern Hemisphere mid-latitude regions that this discrepancy is greatest (see GJ03).

We have evaluated the various solutions by considering the implied ocean heat transport and local comparisons with research buoy measurements. The heat transport evaluations were encouraging for the F1 and F2 solutions as they lead to stronger heat transport in the Northern Hemisphere mid-latitudes which is in better agreement with the imposed constraints and the independent Trenberth residual estimates. However, at a local scale the comparisons with the Subduction Buoy array showed poorer agreement than was found for GJ03 Solution 3 with differences which now exceed 50 Wm^{-2}. Thus, the spatially dependent inverse analysis solutions do not represent a clear improvement on the earlier solutions reported in GJ03.

Further, when one considers the effects of the new shortwave adjustment on the global mean value for this component of the heat exchange an additional problem becomes apparent. Separate comparisons of the original unadjusted SOC shortwave flux with recent satellite based datasets (including estimates from the International Satellite Cloud Climatology Project) reported in Grist and Josey (2004) reveal that the original SOC global mean shortwave flux of 176 Wm^{-2} is slightly smaller than the corresponding satellite value but this difference is only of order 5 Wm^{-2}. With the 6% reduction to the shortwave in GJ03 the global mean becomes 166 Wm^{-2} which is 15 Wm^{-2} smaller than the satellite mean. By comparison, the larger adjustments to the shortwave (up to 18%) found with F1-F3 result in a reduction of 22 Wm^{-2} (Table 3) and hence a global mean of 154 Wm^{-2}. This value is now 27 Wm^{-2} less than the satellite based estimate and it is difficult to see how such a large discrepancy could be accounted for. Given this result, and the Subduction array comparison, we find that our earlier GJ03 Solution 3 adjustment of the SOC climatology is in better agreement with the independent measurements than the spatially dependent solutions. It is thus our preferred means of closing the SOC climatology heat budget imbalance through inverse analysis.

In order to make further progress using spatially dependent inverse analysis techniques additional buoy measurements and heat transport estimates are required. At present there is insufficient information to adequately constrain the fluxes using spatially dependent parameter adjustments while retaining enough independent measurements for their subsequent evaluation. Further advances using inverse analysis will be possible as additional measurements become available in the future e.g. an increase in the number of research buoy deployments is expected as part of the Ocean Observatories Initiative. In addition, the magnitude of the bias which needs to be resolved is expected to be reduced significantly as new flux parameterisations (Josey et al., 2003; Grist and Josey, 2004) developed elsewhere within this COAPEC project are incorporated in the calculation of a revised version of the SOC climatology.

Despite the limitations on further application of the inverse analysis technique at this time, our earlier GJ03 Solution 3 does represent a significant improvement on the original SOC climatology. With this solution the original 30 Wm^{-2} bias has been resolved in a manner which is consistent with our current understanding of the ocean heat transport. Further it is in good

agreement with independent hydrographic and residual technique estimates of the ocean heat transport that were not used in the analysis. We thus believe that it can usefully be employed for forcing ocean models and more generally for studies of ocean-atmosphere interaction.

Note: The GJ03 Solution 3 fields are available to the COAPEC and wider communities from the following website : http://www.soc.soton.ac.uk/JRD/MET/fluxinterim.php.

ACKNOWLEDGEMENTS

The work described in this report has been funded as part of the NERC COAPEC thematic programme under the project: Balancing the Atlantic Heat and Freshwater Budgets, Ref. NER/T/S/2000/00314.

REFERENCES

Aagaard, K. and P. Greisman, 1975: Towards new mass and heat budgets for the Arctic Ocean. *J. Geophys. Res.*, **80**, 3821-3827.

Bacon, S., 1997: Circulation and fluxes in the North Atlantic between Greenland and Ireland. *J. Phys. Oceanogr.,* **27**, 1420-1435.

Bryden, H. L., D. H. Roemmich and J. A. Church, 1991: Ocean heat transport across 24^{O} N in the Pacific. *Deep-Sea Res.,* **38,** 297-324.

da Silva, A. M., C. C. Young and S. Levitus, 1994: Atlas of Surface Marine Data Vol. 1: Algorithms and Procedures. *NOAA Atlas series*, pp.74.

Grist, J. P. and S. A. Josey, 2002: Balancing the SOC Climatology Using Inverse Analysis with Spatially Fixed Parameter Adjustments. Southampton Oceanography Centre Internal Document, No. 80, 38pp. & Figs.

Grist, J. P. and S. A. Josey, 2003: Inverse analysis adjustment of the SOC air-sea flux climatology using ocean heat transport constraints, *J. Climate*, **16,** 3274-3295.

Grist, J. P. and S. A. Josey, 2004: The Impact of Aerosol Loading on Estimates of the Surface Shortwave Flux in the SOC Climatology. Southampton Oceanography Centre Research and Consultancy Report, No. 88, 15pp. & Figs.

Hall, M. M. and H. L. Bryden, 1982: Direct estimates and mechanisms of ocean heat transport. *Deep-Sea Res.*, **29**(3A), 339-359.

Holfort, J. and G. Siedler, 2001: The meridional oceanic transports of heat and nutrients in the South Atlantic. *J. Phys. Oceanogr.*, **31**, 5-29.

Isemer, H.-J., J. Willebrand and L. Hasse, 1989: Fine adjustment of large scale air-sea energy flux parameterizations by direct estimates of ocean heat transport. *J. Clim.*, **2**, 1173-1184.

Josey, S. A., E. C. Kent and P. K. Taylor, 1998: The Southampton Oceanography Centre (SOC) Ocean - Atmosphere Heat, Momentum and Freshwater Flux Atlas. *Southampton Oceanography Centre Report No. 6, Southampton, UK*, 30 pp. & figs.

Josey, S. A., E. C. Kent and P. K. Taylor, 1999: New insights into the ocean heat budget closure problem from analysis of the SOC air-sea flux climatology. *J. Climate*, **12**(9), 2856-2880.

Josey, S. A., R. W. Pascal, P. K. Taylor and M. J. Yelland, 2003: A New Formula For Determining the Atmospheric Longwave Flux at the Ocean Surface at Mid-High Latitudes. Journal of Geophysical Research., **108**(C4) doi:10.1029/2002JC001418.

Klein, B., R. L. Molinari, T. J. Mueller and G. Siedler, 1995: A transatlantic section at 14.5^{O} N: Meridional volume and heat fluxes. *J. Mar. Res.*, **53**, 929-957.

Legler, D. M., 1991: Errors of five-day mean surface wind and temperature conditions due to inadequate sampling. *J. Atmos. Ocean. Tech.,* **8,** 705 - 712.

McDonagh, E. L. and B. A. King, 2004: Oceanic fluxes in the South Atlantic. *J. Phys. Oceanogr.,* submitted.

Moyer, K. A. and R. A. Weller, 1997: Observations of surface forcing from the Subduction Experiment: A comparison with global model products and climatological datasets. *J. Climate,* **10,** 2725-2742.

Roemmich, D. and T. McCallister, 1989: Large scale circulation of the north Pacific. *Prog. Oceanogr.,* **22**, 171-204.

Trenberth, K. E.,, and J. M. Caron, 2001: Estimates of meridional atmosphere and ocean heat transports. *J. Climate,* **14,** 3433-3443.

Speer, K. G, J. Holfort, T. Reynaud, and G. Siedler, 1996: South Atlantic heat transport at 11^{O} S. *The South Atlantic: Present and Past circulation.* Springer, Berlin.

Weller, R. A. and S. P. Anderson, 1996: Surface meteorology and air-sea fluxes in the western equatorial warm pool during the TOGA Coupled Ocean-Atmosphere Response Experiment. *J. Climate,* **9,** 1959-1990.

Weller, R. A., D. L. Rudnick, and N. J. Brink, 1995: Meteorological variability and air-sea fluxes at a closely spaced array of surface moorings. *J. Geophys. Res.,* **100** (C3), 4867-4883.

Weller, R. A, M. F. Baumgartner, S. A. Josey, A. S. Fischer, and J. Kindle, 1998: Atmospheric forcing in the Arabian Sea during 1994-1995: Observations and comparisons with climatology and model. *Deep-Sea Res.,* **45,** 1961-1999.

Wijffels, S. E., J. M. Toole, H. L. Bryden, R. A. Fine, W. J. Jenkins and J. L. Bullister, 1996: The Water Masses and Circulation at 10^{O} N in the Pacific. *Deep-Sea Res.*, **1**, 501-544.

Wijffels, S. E., J. M. Toole, R. Davis, 2001: Revisiting the South Pacific subtropical circulation: A synthesis of World Ocean Circulation Experiment observations along 32^{O} S. *J. Geophys. Res.*, **106**, 19481-19513.

WMO, 1993: International list of selected, supplementary and auxiliary ships. WMO Report, WMO, Geneva, various pagination.

Woodruff, S. D., S. J. Lubker, K. Wolter, S. J. Worley and J. D. Elms, 1993: Comprehensive Ocean-Atmosphere Data Set (COADS) release 1a: 1980-92. *Earth System Monitor*, **4**(1), 4-8.

TABLES

Section	Constraint no. (j)	Heat transport (PW)	Reference
CONVEX Atlantic	1	0.28 ± 0.06	Bacon (1997)
24^{O} N Atlantic	2	1.22 ± 0.30	Hall and Bryden (1982)
14^{O} N Atlantic	3	1.22 ± 0.42	Klein et al. (1995)
8^{O} N Atlantic	4	1.18 ± 0.52	Klein et al. (1995)
11^{O} S Atlantic	5	0.60 ± 0.17	Speer et al. (1996)
30^{O} S Atlantic	6	0.29 ± 0.29	Holfort and Siedler (2001)
A11 Atlantic	7	0.43 ± 0.08	McDonagh and King (2004)
46^{O} N Pacific	8	-0.09 ± 0.30	Roemmich and McCallister (1989)
24^{O} N Pacific	9	0.76 ± 0.30	Bryden et al. (1991)
10^{O} N Pacific	10	0.70 ± 0.50	Wijffels et al. (1996)
65^{O} N Atlantic	Northern Reference	0.1 (exact)	Aagard and Greisman (1975)
66^{O} N Pacific	Northern Reference	0.002 (exact)	Aagard and Greisman (1975)

Table 1. Hydrographic measurements of the heat transport used for the inverse analysis. Note that the errors on the northern reference values are assumed to be sufficiently small that the estimates can be taken to be exact for the purpose of the analysis.

Latitude Band	p_E	p_H	p_S	p_L
1	0.12	0.03	-0.15	0.07
2	0.10	0.01	-0.18	0.05
3	0.09	0.00	-0.16	0.04
4	0.06	0.00	-0.11	0.02
5	0.06	0.00	-0.13	0.03
6	0.06	0.00	-0.13	0.03
7	0.06	0.00	-0.11	0.03
8	0.06	0.00	-0.10	0.03
9	0.07	0.01	-0.12	0.04
10	0.04	0.00	-0.08	0.03
11	0.02	0.00	-0.05	0.02
Area-weighted mean	0.07	0.01	-0.12	0.03
GJ03 Solution 3	0.19	0.07	-0.06	0.09

Table 2. Fractional adjustments to the inverse analysis parameters associated with each latitude band for F1. Also shown are the area weighted mean adjustments $\langle p_E \rangle$, $\langle p_H \rangle$, $\langle p_S \rangle$ and $\langle p_L \rangle$ where for example, $\langle p_E \rangle = \sum A_i p_{Ei} / \sum A_i$, and the sum is over all the latitude bands, each of which has area A_i . In addition, the globally fixed inverse analysis parameter adjustments from GJ03 Solution 3 are tabulated for comparison.

	Q_E	Q_H	Q_S	Q_L
GJ03 Solution 3	-17	-1	-10	-4
F1 (raw)	-6	0	-22	-2
F1 (smoothed)	-6	0	-22	-2
F2a ($0.2<e_i<0.3$)	-6	0	-22	-2
F2b ($0.1<e_i<0.3$)	-6	0	-23	-2
F3c ($0.24 < e_i< 0.36$)	-6	0	-22	-2

Table 3. Global mean adjustments to the component fluxes of the original SOC climatology for GJ03 Solution 3, F1 (raw), F1 (smoothed), F2a, F2b and F3c. Units are Wm^{-2}.

Latitude Band	Solution 3 - SOC	F1 raw – SOC	F1 smoothed – SOC	F2a smoothed - SOC ($0.2<e_i<0.3$)	F2b smoothed - SOC ($0.1<e_i<0.3$)	F3c smoothed – SOC ($0.24<e_i<0.36$)
1	-22	-27	-28	-28	-26	-26
2	-36	-45	-45	-45	-47	-45
3	-40	-47	-45	-45	-46	-40
4	-38	-32	-33	-32	-34	-37
5	-36	-35	-35	-35	-36	-31
6	-38	-37	-36	-36	-40	-30
7	-41	-31	-31	-29	-28	-29
8	-38	-28	-28	-27	-31	-28
9	-32	-28	-27	-31	-31	-24
10	-24	-14	-14	-17	-16	-23
11	-17	-7	-8	-9	-7	-18
Global	-32	-30	-30	-30	-31	-30

Table 4. The difference of the area average adjusted net heat flux from the original SOC climatology (per latitude band) for: GJ03 Solution 3, F1 raw, F1 smoothed, F2a, F2b and F3c. Units are Wm^{-2}.

Subduction Array (18-33º N, 22-34 º W)

	Latent	Sensible	Shortwave	Longwave	Net
Buoy	-103	-7	209	-62	37
SOC	-108	-7	200	-56	29
(SOC - buoy)	(-5)	(0)	(-9)	(6)	(-8)
S3	-129	-7	189	-61	-8
(S3 - buoy)	(-26)	(0)	(-20)	(1)	(-45)
F1	-118	-7	168	-61	-18
(F1 – buoy)	(-15)	(0)	(-41)	(1)	(-55)
F2a	-118	-7	168	-59	-16
(F2a – buoy)	(-15)	(0)	(-41)	(3)	(-53)
F2b	-118	-7	167	-59	-17
(F2b –buoy)	(-15)	(0)	(-42)	(3)	(-52)
F3c	-116	-7	174	-58	-7
(F3c – buoy)	(-13)	(0)	(-35)	(4)	(-44)

Table 5a. Deployment average values of the various heat flux components and the net heat flux for the Subduction Array (Buoy, averaged over all buoys in the array), the original SOC climatology (SOC) and the climatology adjusted according to Solution 3 of GJ03 (S3), F1, F2a, F2b, and F3c. Units are Wm^{-2}.

Arabian Sea Buoy (15.5ºN, 61.5ºE)

	Latent	Sensible	Shortwave	Longwave	Net
Buoy	-121	-2	243	-59	61
SOC	-110	-1	240	-51	78
(SOC - buoy)	(11)	(1)	(-3)	(8)	(17)
S3	-131	-1	226	-56	38
(S3 - buoy)	(-10)	(1)	(-17)	(3)	(-23)
F1	-118	-1	207	-55	33
(F1 – buoy)	(3)	(1)	(-36)	(4)	(-28)
F2a	-117	-1	207	-53	36
(F2a – buoy)	(4)	(1)	(-36)	(6)	(-25)
F2b	-118	-1	207	-53	35
(F2b –buoy)	(3)	(1)	(-36)	(6)	(-26)
F3	-114	-1	225	-52	58
(F3 – buoy)	(7)	(1)	(-18)	(7)	(-3)

Table 5b. Deployment average values of the various heat flux components and the net heat flux for the Arabian Sea buoy (Buoy), the original SOC climatology (SOC) and the climatology adjusted according to Solution 3 of GJ03 (S3), F1, F2a, F2b, and F3c. Units are Wm^{-2}.

TOGA-COARE buoy (1.75ºS, 156ºE)

	Latent	Sensible	Shortwave	Longwave	Net
Buoy	-108	-9	196	-58	21
SOC	-115	-10	219	-50	44
(SOC - buoy)	(-7)	(-1)	(23)	(8)	(23)
S3	-136	-10	208	-54	8
(S3 - buoy)	(-28)	(-1)	(12)	(4)	(-13)
F1	-121	-9	192	-53	9
(F1 – buoy)	(-13)	(0)	(-4)	(5)	(-12)
F2a	-121	-9	191	-51	10
(F2a – buoy)	(-13)	(0)	(-5)	(7)	(-11)
F2b	-122	-9	189	-52	6
(F2b –buoy)	(-14)	(0)	(-7)	(6)	(-15)
F3	-119	-9	204	-51	25
(F3 – buoy)	(-11)	(0)	(8)	(7)	(4)

Table 5c. Deployment average values of the various heat flux components and the net heat flux for the TOGA-COARE buoy (Buoy), the original SOC climatology (SOC) and the climatology adjusted according to Solution 3 of GJ03 (S3), F1, F2a, F2b, and F3c. Units are Wm^{-2}.

FASINEX array (27°N, 70°W)

	Latent	Sensible	Shortwave	Longwave	Latent + Sensible + Shortwave
Buoy	-170	-17	222	---	35
SOC	-125	-10	220	-63	85
(SOC - buoy)	(45)	(7)	(-2)	(---)	(50)
S3	-149	-11	208	-69	48
(S3 - buoy)	(21)	(6)	(-14)	(---)	(13)
F1	-137	-10	183	-69	36
(F1 – buoy)	(33)	(7)	(-39)		(1)
F2a	-138	-10	182	-66	34
(F2a – buoy)	(32)	(7)	(-40)		(-1)
F2b	-138	-10	181	-66	(33)
(F2b –buoy)	(32)	(7)	(-41)		(-2)
F3	-143	-10	169	-68	16
(F3 – buoy)	(27)	(7)	(-53)		(-19)

Table 5d. Deployment average values of the various heat flux components and the net heat flux for the FASINEX Array (Buoy), the original SOC climatology (SOC) and the climatology adjusted according to Solution 3 of GJ03 (S3), F1, F2a, F2b, and F3c. Note that longwave measurements were not made on this deployment and that the final column shows the sum of the latent, sensible and shortwave fluxes. Units are Wm^{-2}.

FIGURE CAPTIONS

Fig. 1 a) The eleven latitude bands used in F1 and F2. b) The surface area of the ocean within each of the eleven latitude bands.

Fig. 2) The variation of the parameter error (e_i) with latitude band as prescribed for F2. The green solid line denotes the parameter error varying from 0.2 in the Northern Hemisphere to 0.3 in the Southern Hemisphere (F2a). The green dashed line denotes the parameter error varying from 0.1 in the Northern Hemisphere to 0.3 in the Southern Hemisphere (F2b). The solid black line is the latitudinal variation of $1/\gamma$, where γ is the square root of the zonally averaged observation density for January 1986. Observation density is the number of observations per 1-degree grid cell.

Fig. 3) Square root of the density of observations per 1-degree grid cell for January 1986.

Fig. 4 a – d) Areas 1 - 4 (shown with black shading) used in the inverse analysis for F3. The areas are defined by the square root of the number of observations in each 1-degree grid cell in January 1986.

Fig. 4 e – h) Areas 5 - 8 (shown with black shading) used in the inverse analysis for F3. The areas are defined by the square root of the number of observations in each 1-degree grid cell in January 1986.

Fig. 4 i – k) Areas 9 - 11 (shown with black shading) used in the inverse analysis for F3. The areas are defined by the square root of the number of observations in each 1-degree grid cell in January 1986.

Fig. 5) Area (m^2) of the eleven regions defined by observation density in F3.

Fig. 6) Parameter adjustments for the F1 inverse analysis solution. The unsmoothed solution is denoted by a solid line in each case and the interpolated solution by a dash-dot line. The number of the latitude band (as defined in Fig. 1a) is denoted by the bold text. The parameter errors were globally fixed at 0.2. The thick lines on the right hand axis denote the spatially fixed parameter adjustments from GJ03 Solution 3.

Fig. 7 a – e) Fields showing the unsmoothed inverse analysis adjustments of the component and net heat fluxes for Solution F1. The global mean adjustments are denoted above each panel; f) the unsmoothed adjusted net heat flux field for F1, in this case the global mean net heat flux is denoted above the panel.

Fig. 8) The difference between the area averaged adjusted net heat flux from the original SOC climatology (per latitude band) and a) GJ03 Solution 3, b) F1 unsmoothed, c) F1 smoothed, d) F2a, e) F2b and f) F3c. The units are Wm^{-2}.

Fig. 9 a – e) Fields showing the smoothed inverse analysis adjustments of the component and net heat fluxes for Solution F1. The global mean adjustments are denoted above each panel; f) the smoothed adjusted net heat flux field for F1, in this case the global mean net heat flux is denoted above the panel.

Fig. 10) The difference in the net heat flux field between a) F1 and GJ03 Solution 3, b) F2a and F1, c) F2b and F1, d) F3c and F1; e) the zonally averaged net heat flux adjustments from the original SOC climatology for GJ03 Solution 3, F1, F2a and F3c.

Fig. 11) Parameter adjustments for the inverse analysis solutions using 6, 11 (F1) and 16 latitude bands. The black dotted lines denote the parameter error.

Fig. 12) Parameter adjustments for the F2a inverse analysis solution (solid coloured lines). The number of the latitude band is denoted in bold text. Dash-dot lines are the solution for F1. The parameter errors for F2a are indicated by the black solid lines.

Fig. 13 a – e) Fields showing the inverse analysis adjustments of the component and net heat fluxes for Solution F2a. The global mean adjustments are denoted above each panel; f) the adjusted net heat flux field for F2a, in this case the global mean net heat flux is denoted above the panel.

Fig. 14) Parameter adjustments for the F2b inverse analysis solution (solid coloured lines). The number of the latitude band is denoted in bold text. Dash-dot lines are the solution for F2a. The parameter errors for F2b are indicated by the black solid lines.

Fig. 15) Parameter adjustments for the F3a, F3b and F3c inverse analysis solutions (solid coloured lines). The dashed lines are the parameter errors for the formulation of the corresponding colour. The number of the region as defined by Fig. 4 is denoted by the bold text on the x-axis; a) p_E, b) p_H, c) p_S and d) p_L.

Fig. 16 a – e) Fields showing the inverse analysis adjustments of the component and net heat fluxes for Solution F3c. The global mean adjustments are denoted above each panel; f) the adjusted net heat flux field for F3c, in this case the global mean net heat flux is denoted above the panel.

Fig. 17) The difference (climatology – hydrography) between area-averaged net heat flux values from the SOC climatology and hydrography for a) the original SOC climatology, b) the SOC climatology adjusted according to GJ03 Solution 3, c) the SOC climatology adjusted according to F1, d) the SOC climatology adjusted according to F2a and e) the SOC climatology adjusted according to F3c. Units are Wm^{-2}.

Fig. 18) Ocean heat transport as calculated from various climatologies: SOC GJ03 Solution 3 (solid black line), Trenberth residual (dashed black line), F1 (solid red line), F2a (solid green line) and F3c (solid magenta line), for a) the Atlantic Ocean, b) the Pacific Ocean and c) the Global Ocean. The black crosses indicate hydrographic estimates of the heat transport that were used in the inverse analysis, the red cross is a more recent estimate based on Wijffels et al. (2001).

Fig. 19) Summary plot showing the difference (Q) between SOC estimates and WHOI research buoy measurements of heat flux components and the net heat flux for various buoy deployments. White bars: differences between the original SOC climatology and the buoys. Black bars: differences between GJ03 Solution 3 and the buoys. Red bars: differences between F1 and the buoys. Green bars: differences between F2a and the buoys. Magenta bars: differences between F3c and the buoys. The abbreviations refer to the different buoys considered as follows: Sub. refers to the mean of the Subduction Buoy array; A. Sea to the Arabian Sea buoy; TOGA to the TOGA-COARE buoy; and FAS. to the mean of the FASINEX buoy array. Note that buoy measurements of the longwave were not available for FASINEX and that in this case the net heat flux differences are an approximation based on the sum of the latent, sensible and shortwave fluxes.

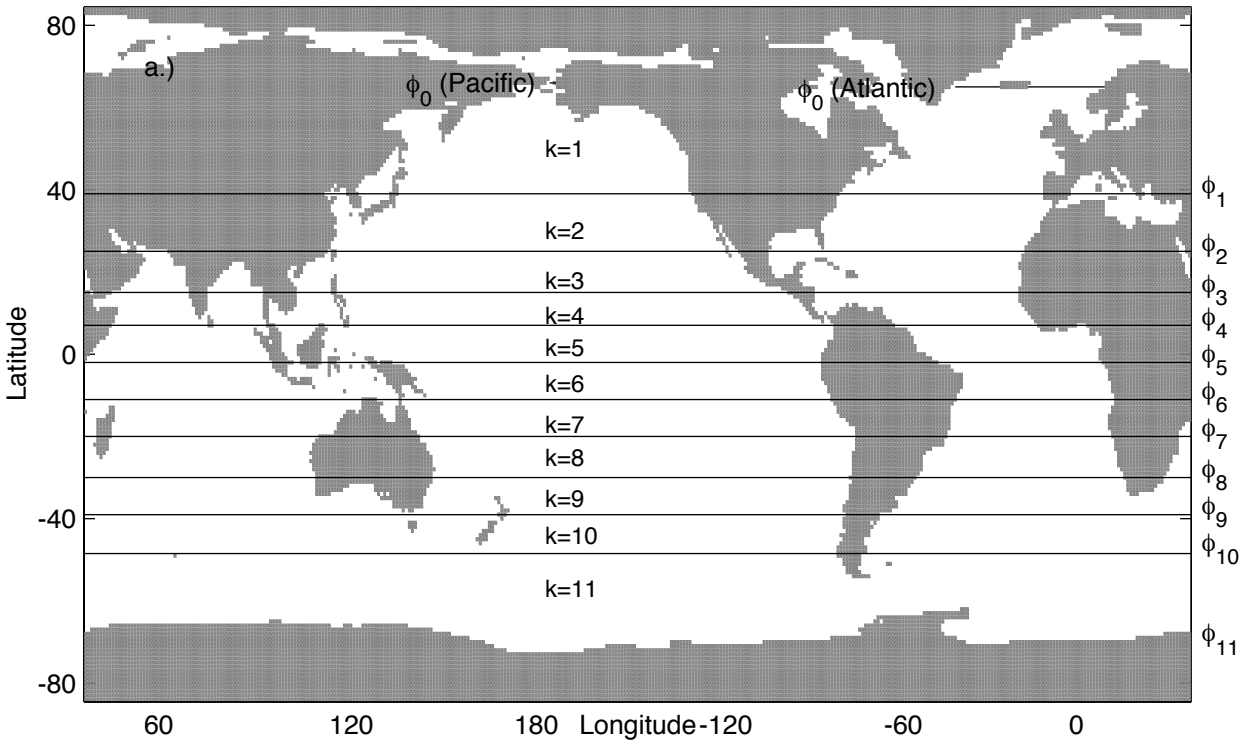

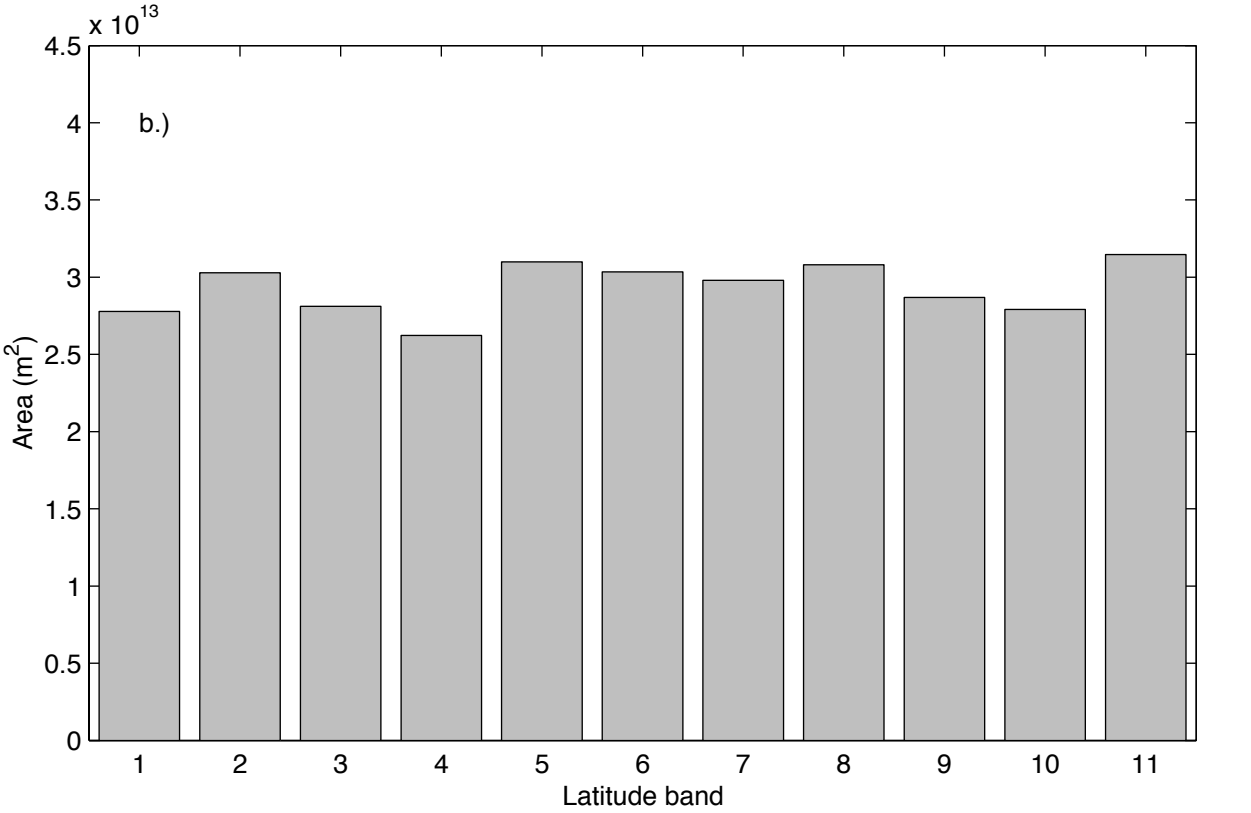

Fig. 1 a) The eleven latitude bands used in F1 and F2. b) The surface area of the ocean within each of the eleven latitude bands.

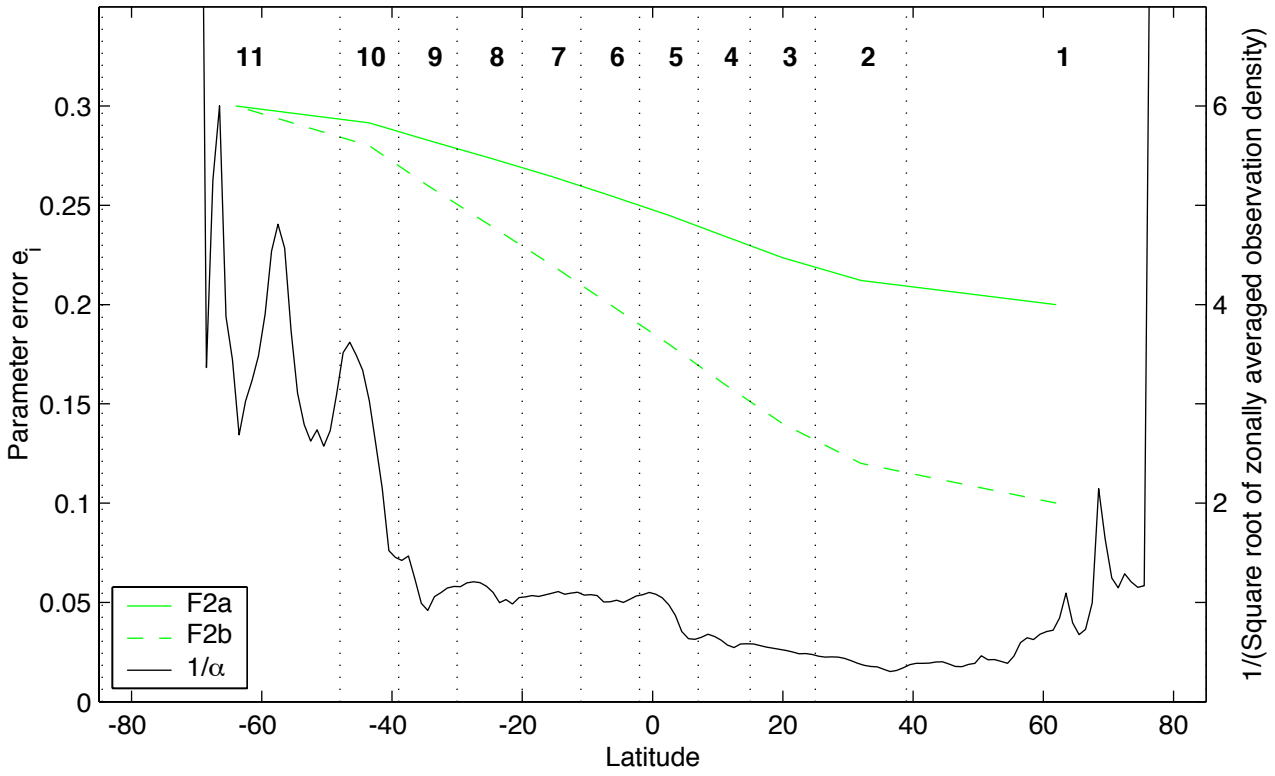

Fig. 2) The variation of the parameter error (e_i) with latitude band as prescribed for F2. The green solid line denotes the parameter error varying from 0.2 in the Northern Hemisphere to 0.3 in the Southern Hemisphere (F2a). The green dashed line denotes the parameter error varying from 0.1 in the Northern Hemisphere to 0.3 in the Southern Hemisphere (F2b). The solid black line is the latitudinal variation of $1/\alpha$, where α is the square root of the zonally averaged observation density for January 1986. Observation density is the number of observations per 1-degree grid cell.

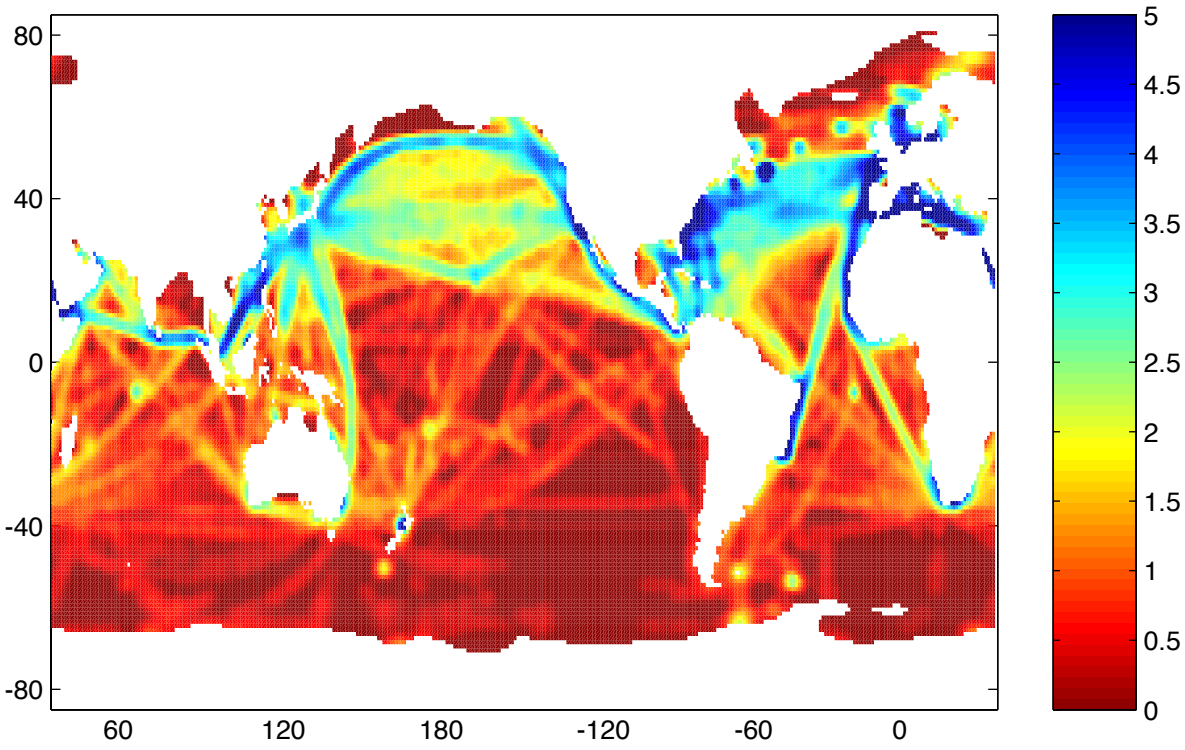

Fig. 3) Square root of the density of observations per 1-degree grid cell for January 1986.

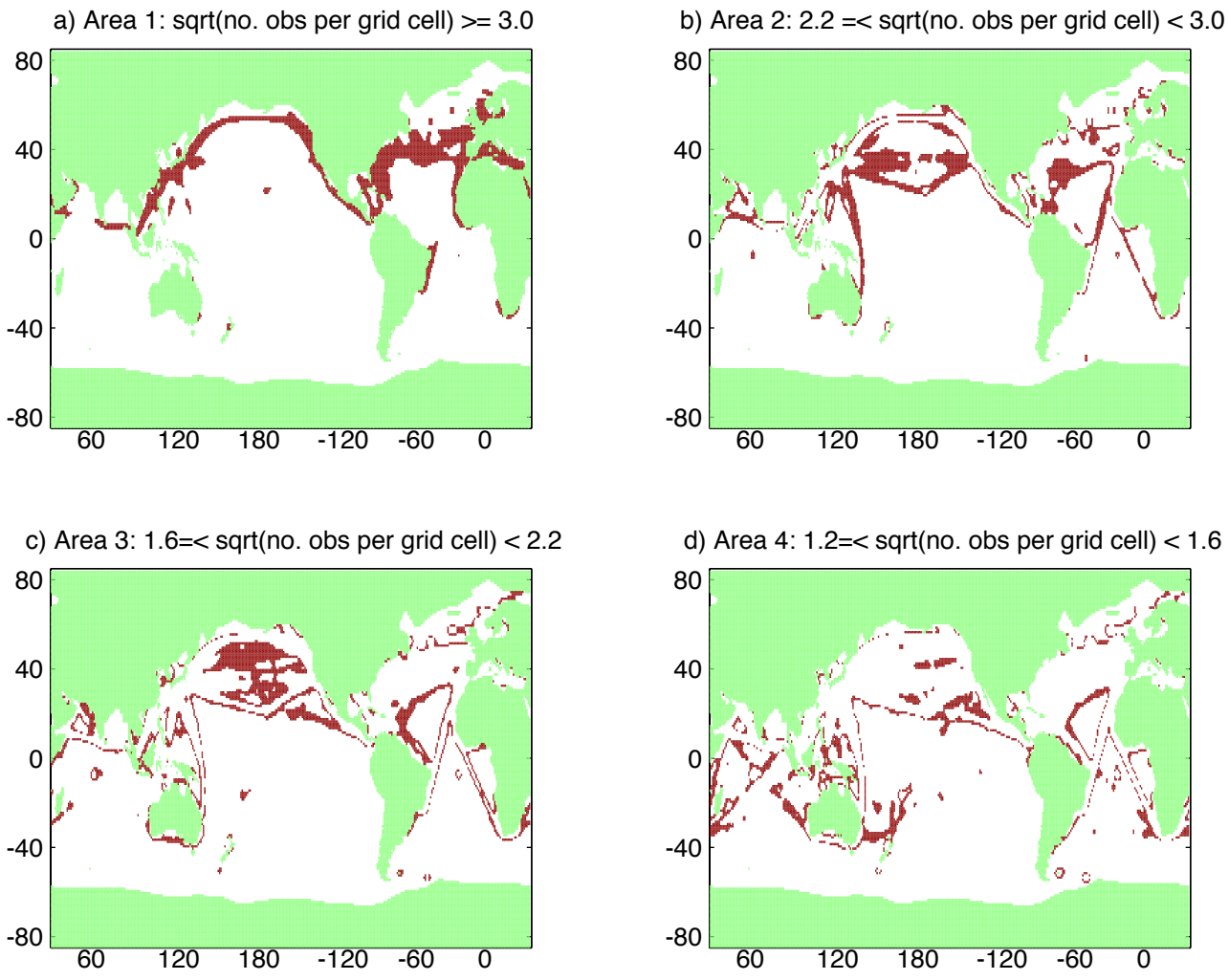

Fig. 4 a - d) Areas 1 - 4 (shown with black shading) used in the inverse analysis for F3. The areas are defined by the square root of the number of observations in each 1-degree grid cell in January 1986.

e) Area 5: 0.95 =< sqrt(no. obs per grid cell) < 1.2

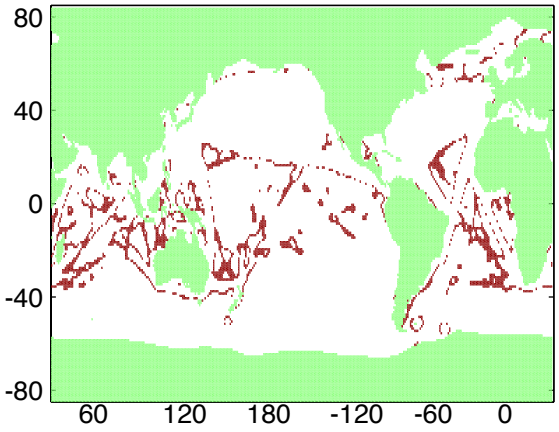

f) Area 6: 0.75 =< sqrt(no. obs per grid cell) < 0.95

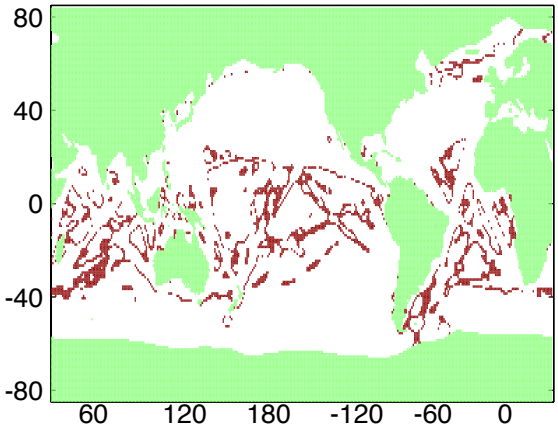

g) Area 7: 0.6 =< sqrt(no. obs per grid cell) < 0.75

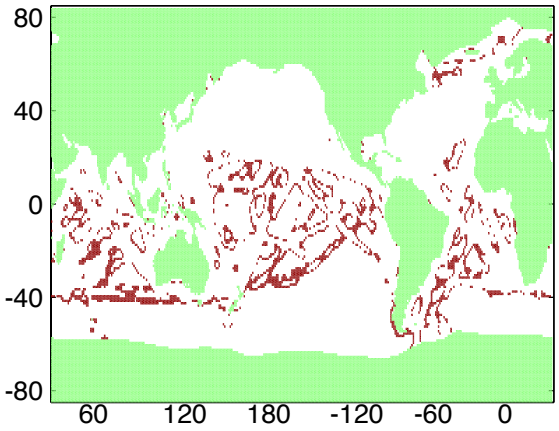

h) Area 8: 0.45=< sqrt(no. obs per grid cell) < 0.6

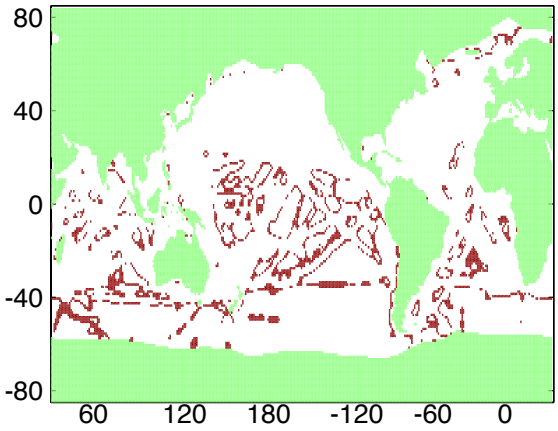

Fig. 4 e - h) Areas 5 - 8 (shown with black shading) used in the inverse analysis for F3. The areas are defined by the square root of the number of observations in each 1-degree grid cell in January 1986.

i) Area 9: 0.25 =< sqrt(no. obs per grid cell) < 0.45

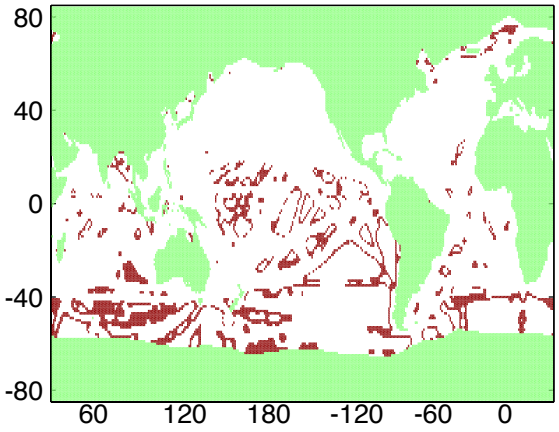

j) Area 10: 0.03 =< sqrt(no. obs per grid cell) < 0.25

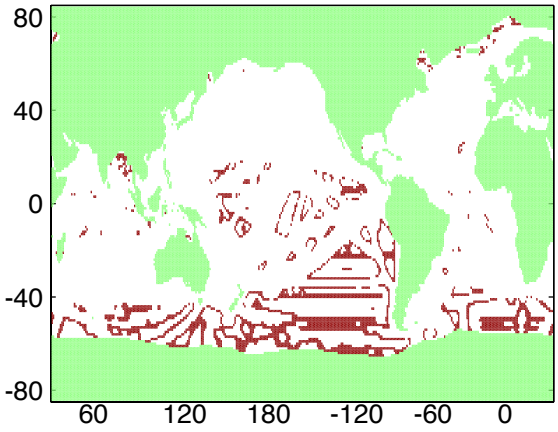

k) Area 11: sqrt(no. obs per grid cell) < 0.03

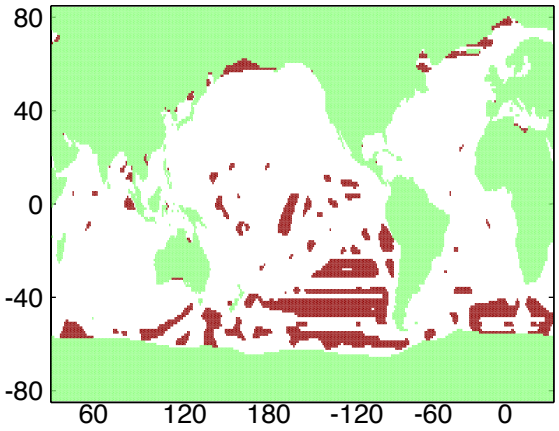

Fig. 4 i - k) Areas 9 - 11 (shown with black shading) used in the inverse analysis for F3. The areas are defined by the square root of the number of observations in each 1-degree grid cell in January 1986.

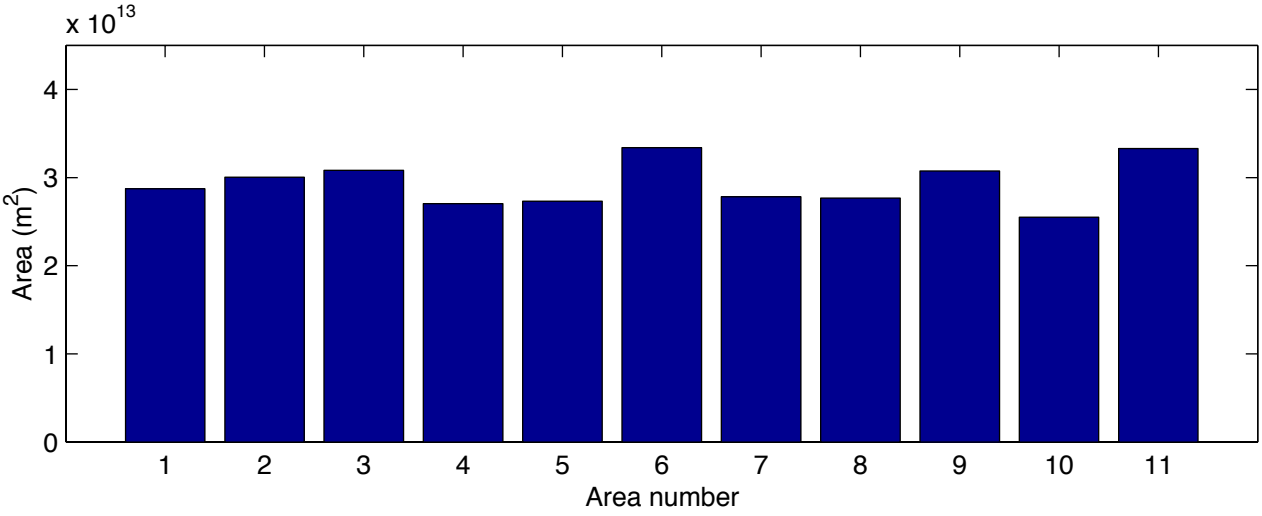

Fig. 5) Area (m^2) of the eleven regions defined by observation density in F3.

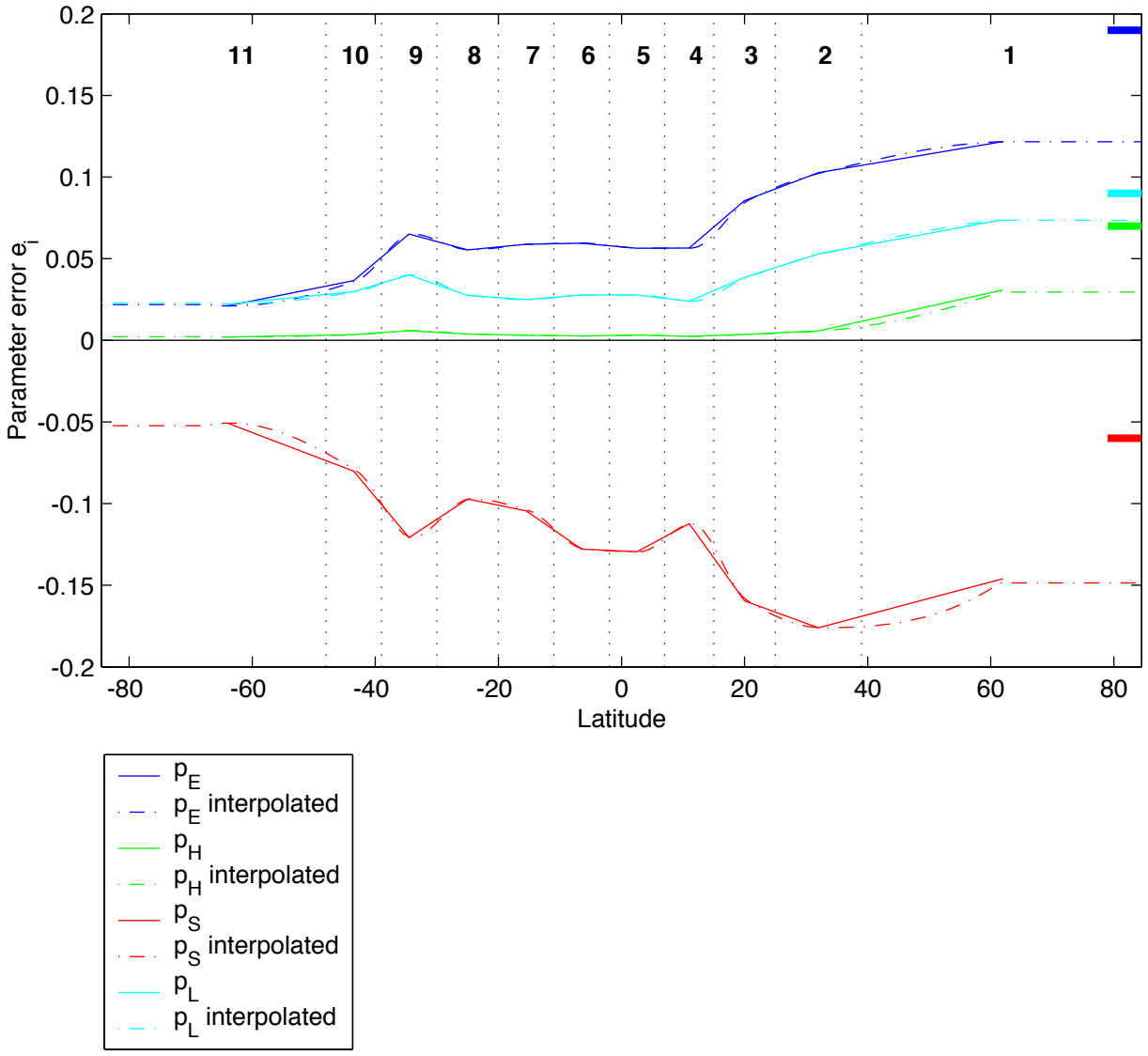

Fig. 6) Parameter adjustments for the F1 inverse analysis solution. The unsmoothed solution is denoted by a solid line in each case and the interpolated solution by a dash-dot line. The number of the latitude band (as defined in Fig. 1a) is denoted by the bold text. The parameter errors were globally fixed at 0.2. The thick lines on the right hand axis denote the spatially fixed parameter adjustments from GJ03 Solution 3.

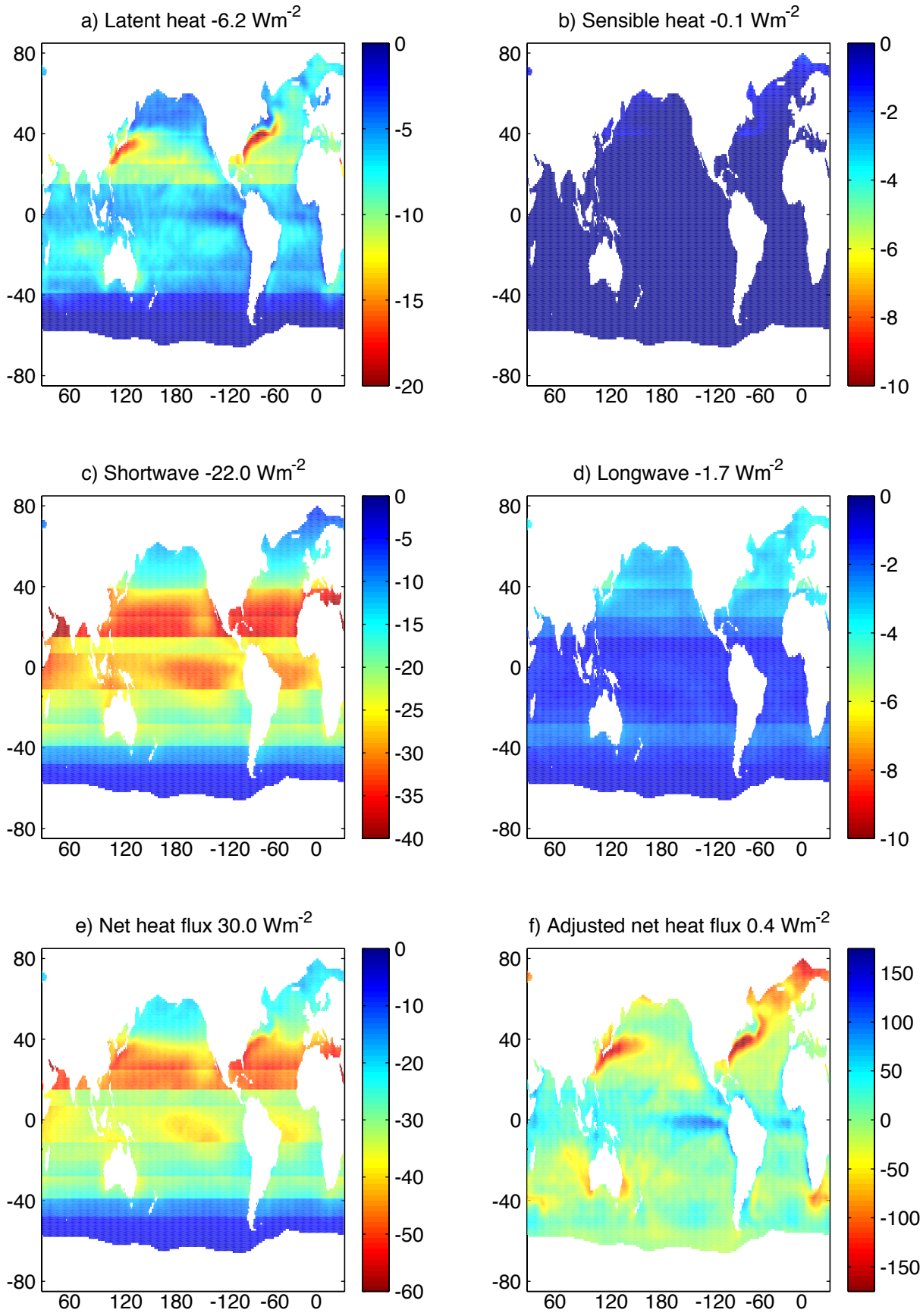

Fig. 7 a - e) Fields showing the unsmoothed inverse analysis adjustments of the component and net heat fluxes for Solution F1. The global mean adjustments are denoted above each panel; f) the unsmoothed adjusted net heat flux field for F1, in this case the global mean net heat flux is denoted above the panel.

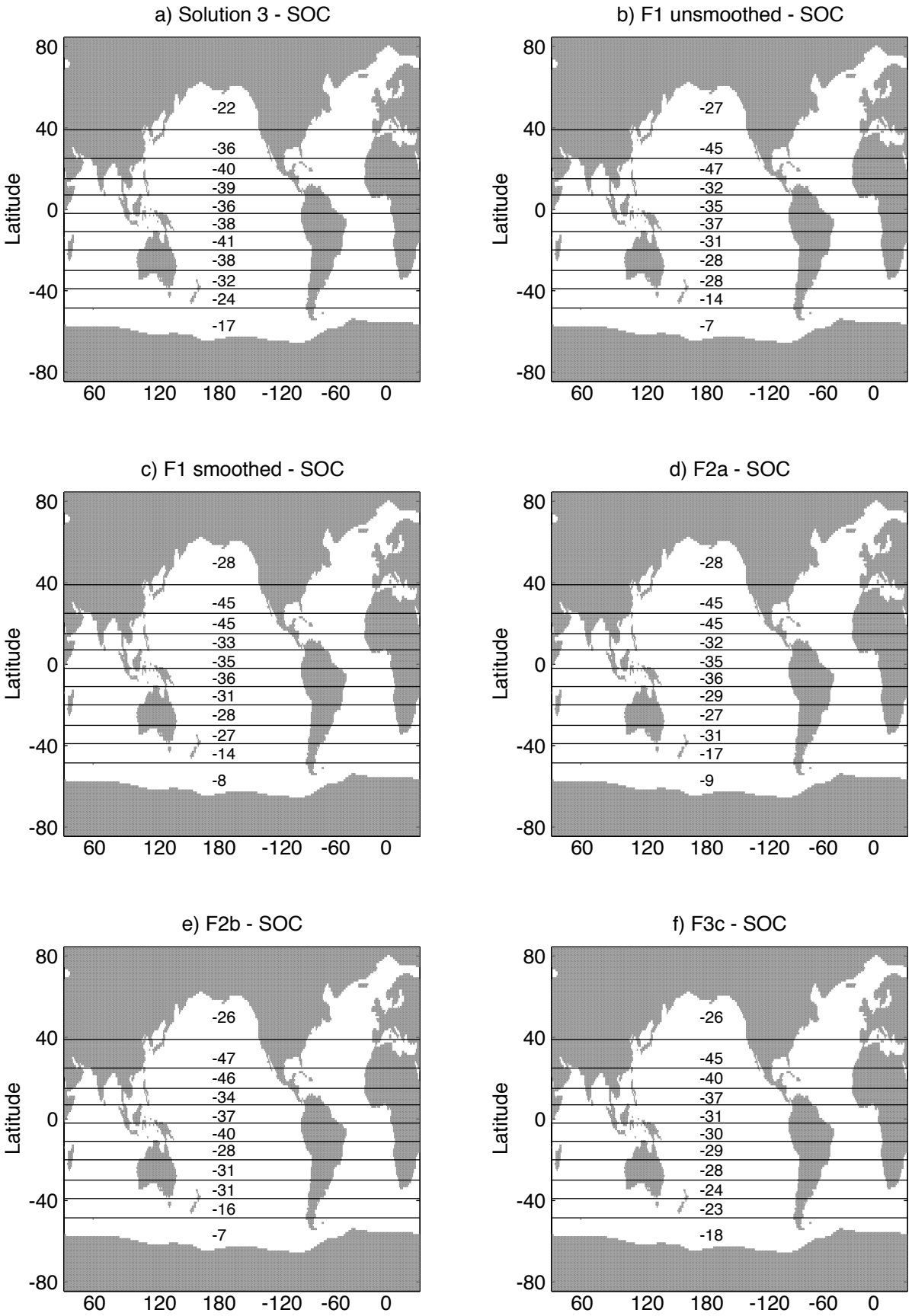

Fig. 8) The difference between the area averaged adjusted net heat flux from the original SOC climatology (per latitude band) and a) GJ03 Solution 3, b) F1 unsmoothed, c) F1 smoothed, d) F2a, e) F2b and f) F3c. The units are Wm^{-2}.

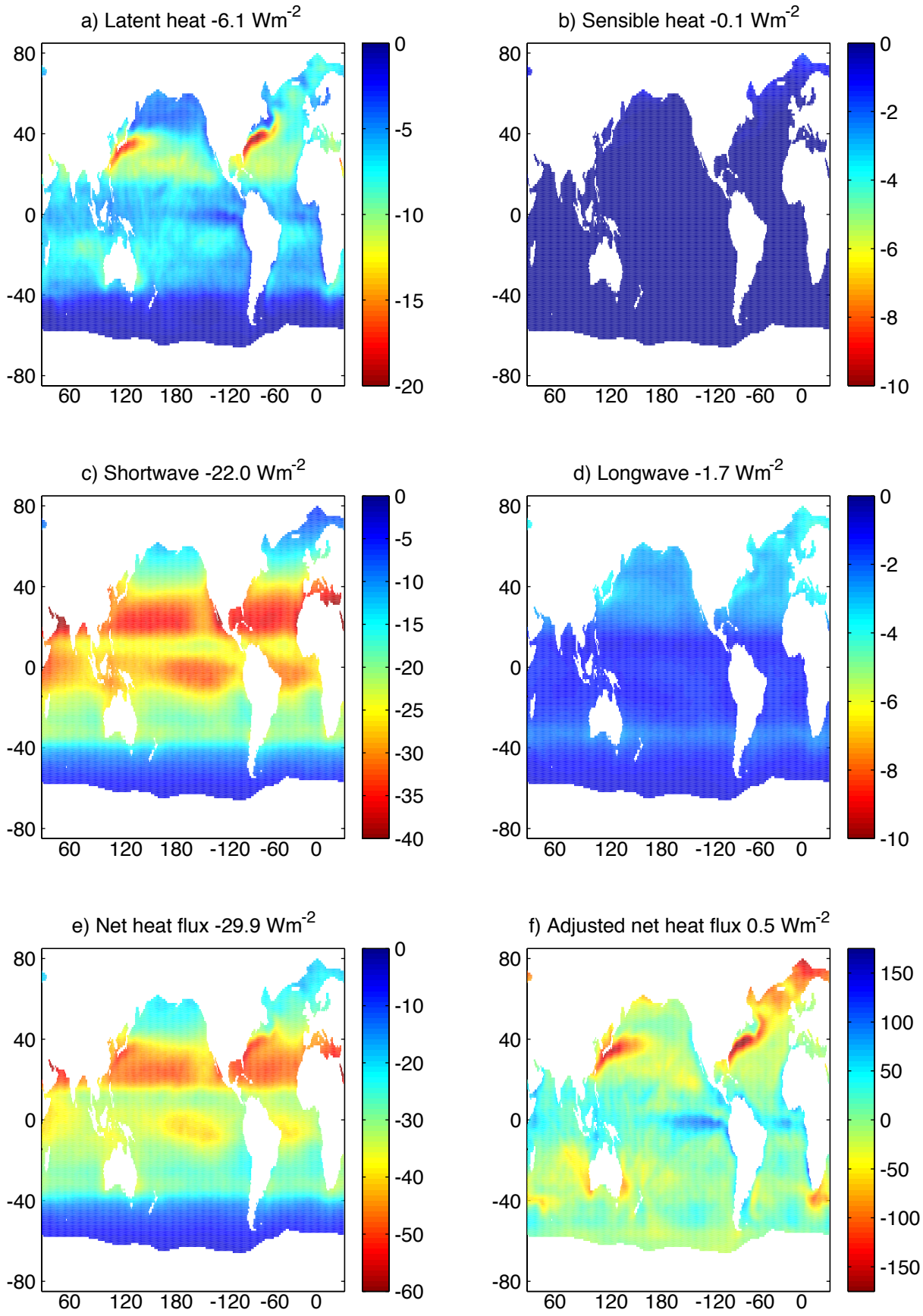

Fig. 9 a - e) Fields showing the smoothed inverse analysis adjustments of the component and net heat fluxes for Solution F1. The global mean adjustments are denoted above each panel; f) the smoothed adjusted net heat flux field for F1, in this case the global mean net heat flux is denoted above the panel.

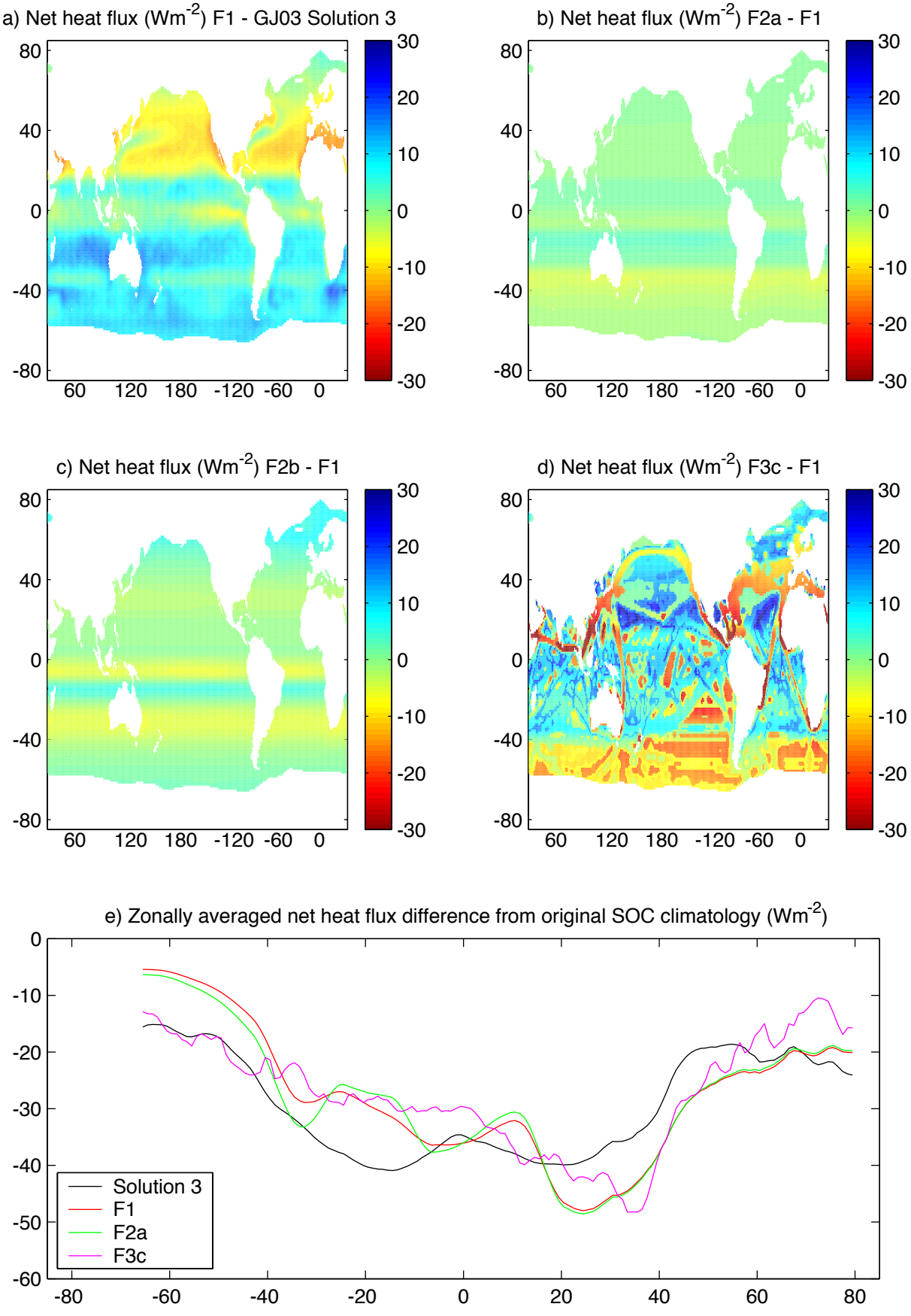

Fig. 10) The difference in the net heat flux field between a) F1 and GJ03 Solution 3, b) F2a and F1, c) F2b and F1, d) F3c and F1; e) the zonally averaged net heat flux adjustments from the original SOC climatology for GJ03 Solution 3, F1, F2a and F3c.

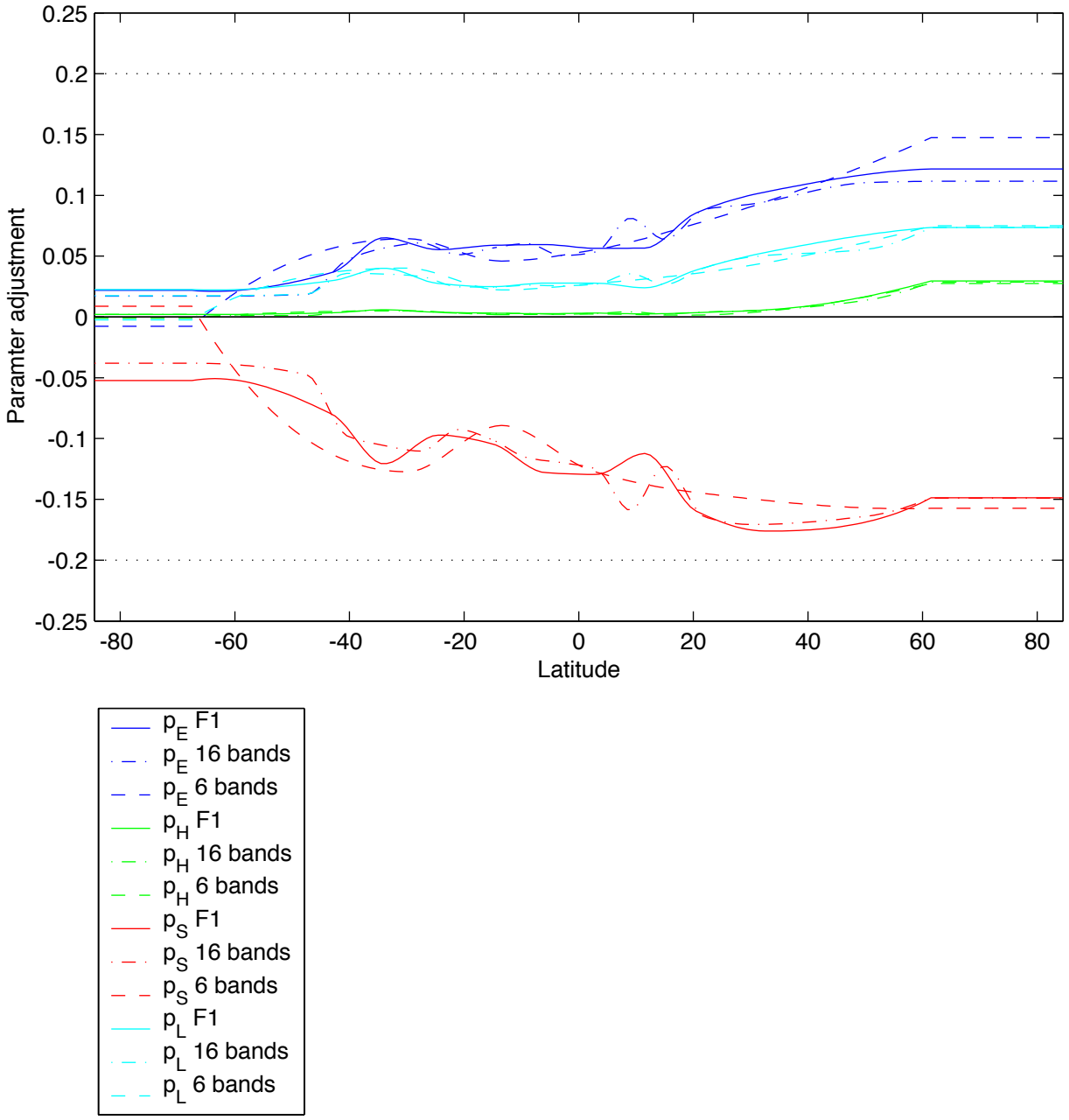

Fig. 11) Parameter adjustments for the inverse analysis solutions using 6, 11 (F1) and 16 latitude bands. The black dotted lines denote the parameter error.

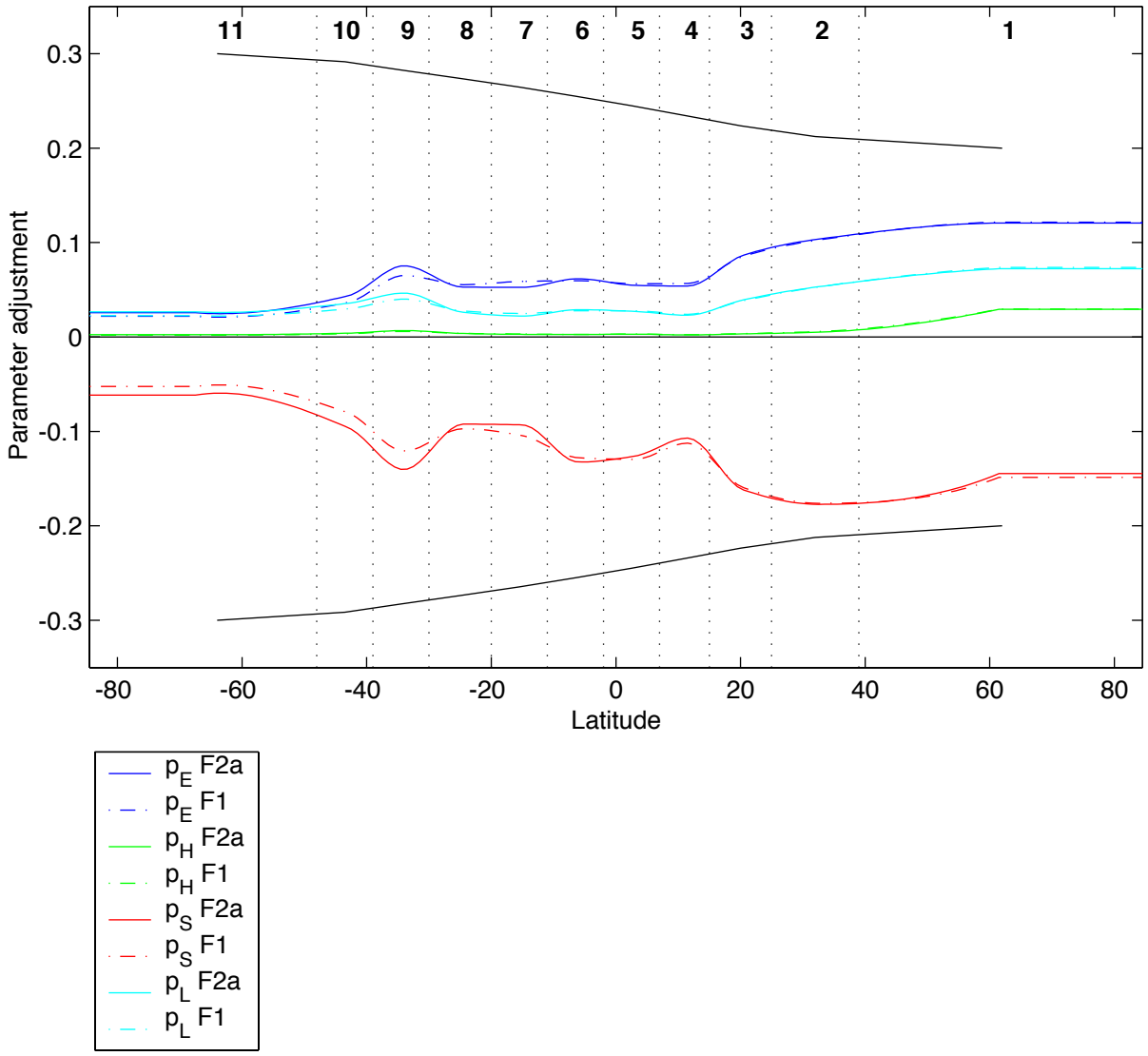

Fig. 12) Parameter adjustments for the F2a inverse analysis solution (solid coloured lines). The number of the latitude band is denoted in bold text. Dash-dot lines are the solution for F1. The parameter errors for F2a are indicated by the black solid lines.

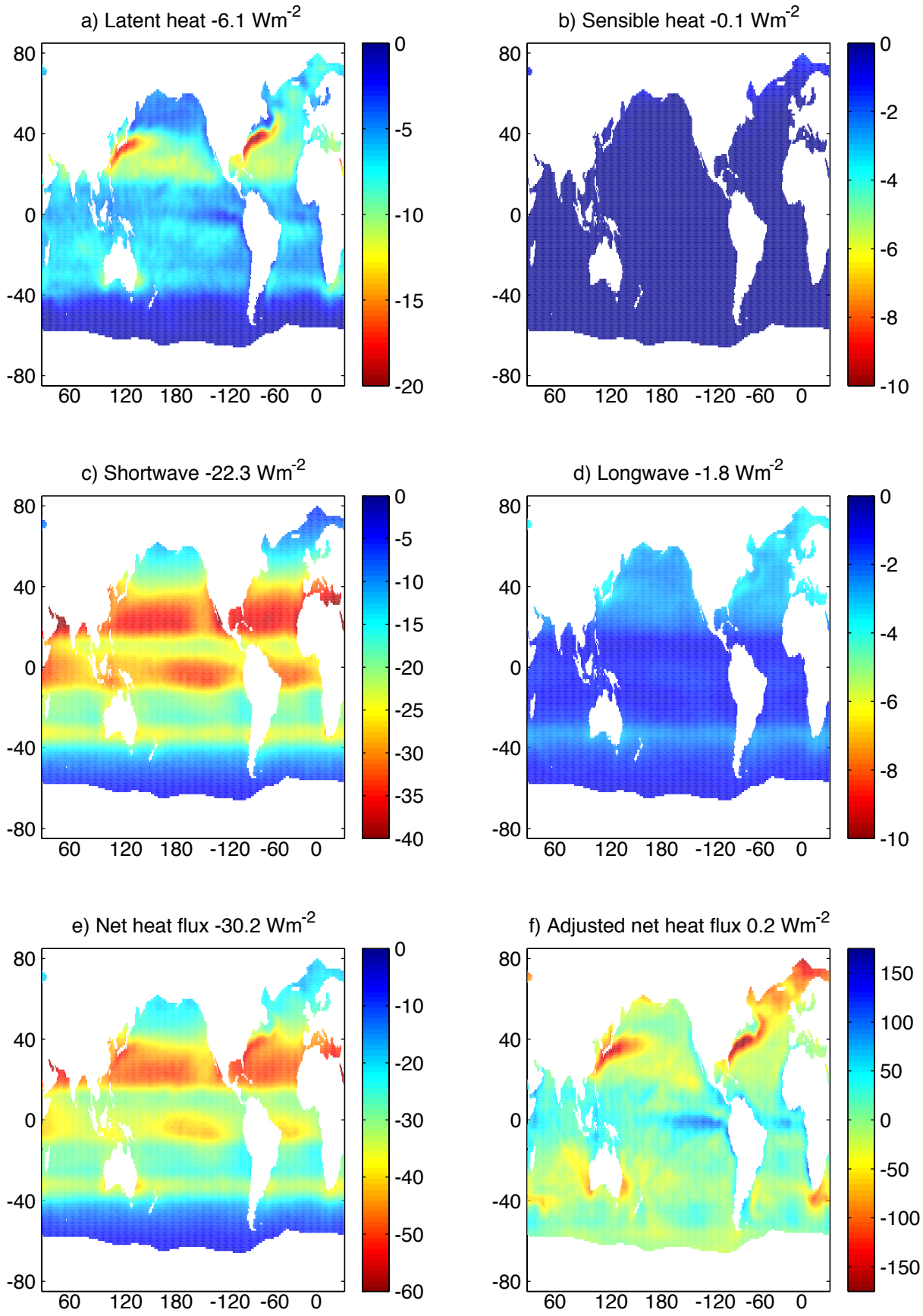

Fig. 13 a - e) Fields showing the inverse analysis adjustments of the component and net heat fluxes for Solution F2a. The global mean adjustments are denoted above each panel; f) the adjusted net heat flux field for F2a, in this case the global mean net heat flux is denoted above the panel.

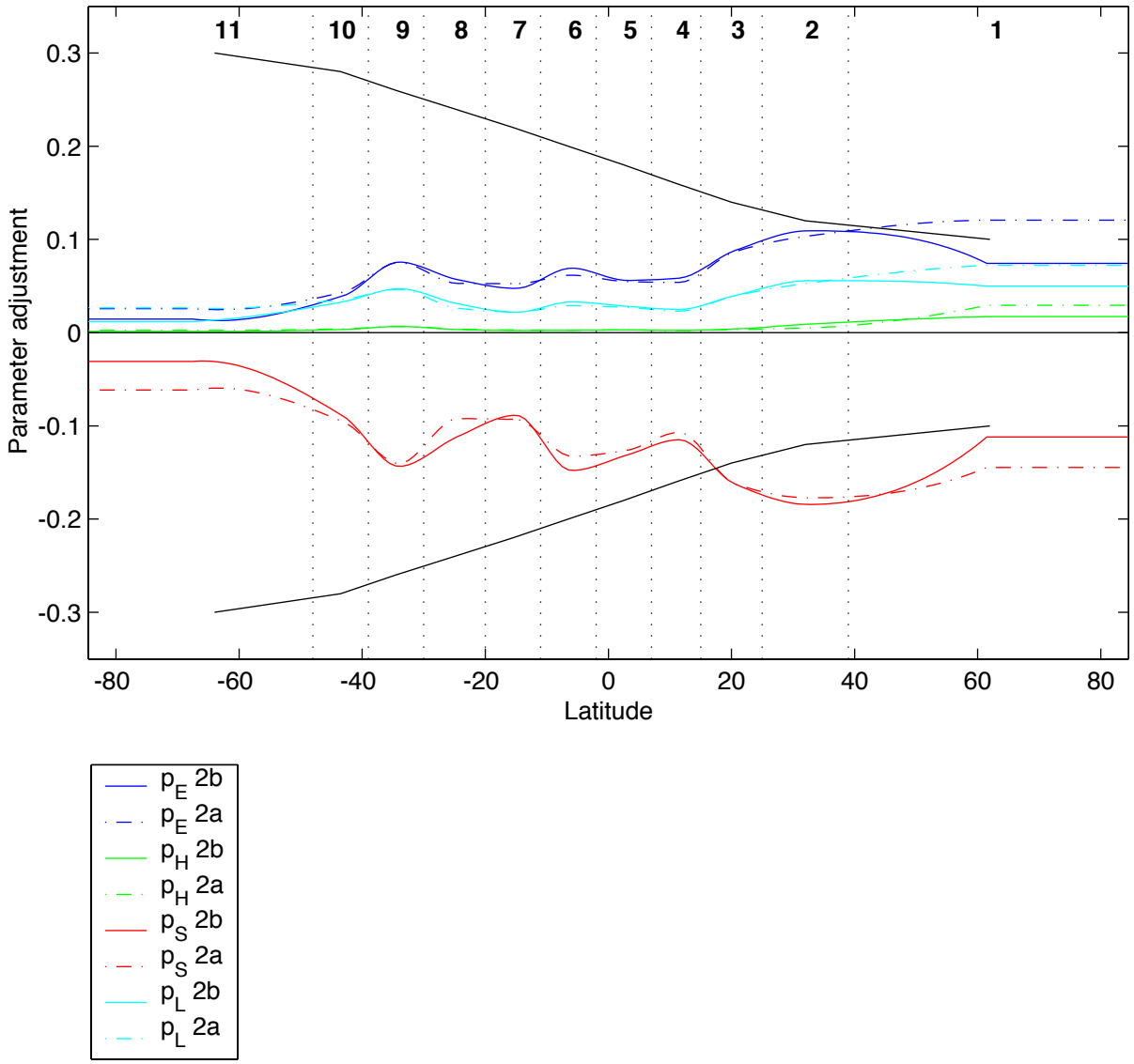

Fig. 14) Parameter adjustments for the F2b inverse analysis solution (solid coloured lines). The number of the latitude band is denoted in bold text. Dash-dot lines are the solution for F2a. The parameter errors for F2b are indicated by the black solid lines.

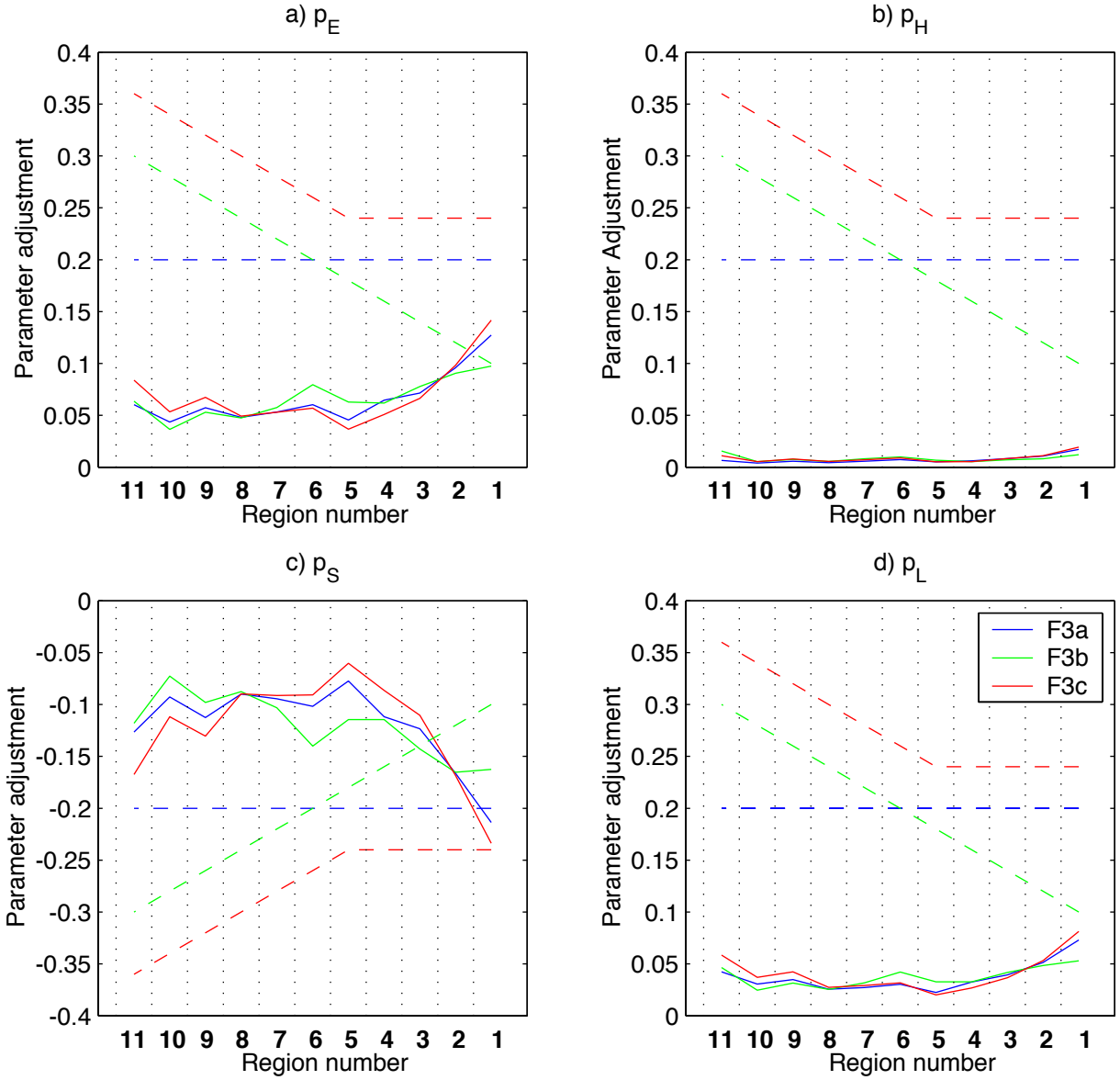

Fig. 15) Parameter adjustments for the F3a, F3b and F3c inverse analysis solutions (solid coloured lines). The dashed lines are the parameter errors for the formulation of the corresponding colour. The number of the region as defined by Fig. 4 is denoted by the bold text on the x-axis; a) p_E, b) p_H, c) p_S and d) p_L.

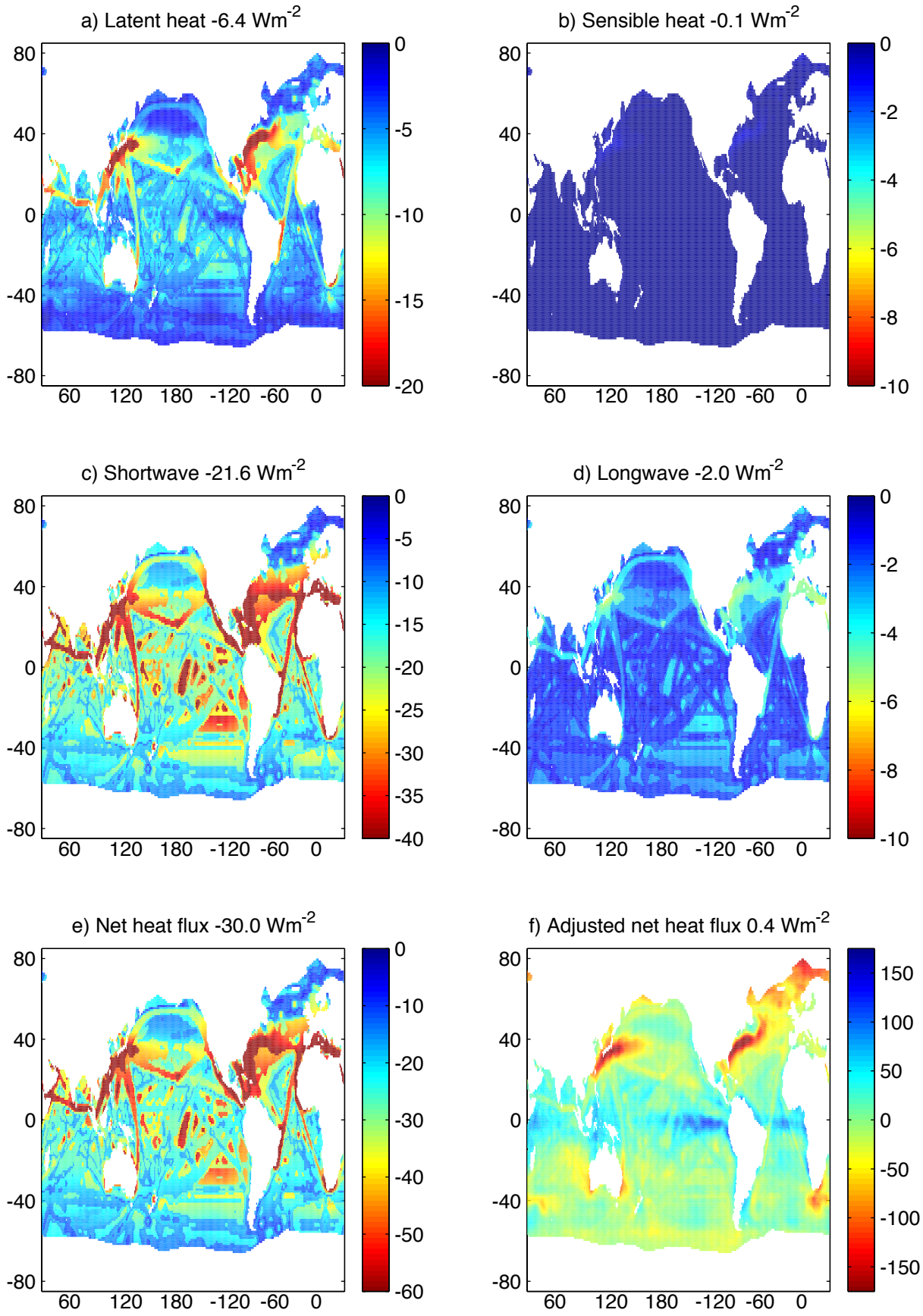

Fig. 16 a - e) Fields showing the inverse analysis adjustments of the component and net heat fluxes for Solution F3c. The global mean adjustments are denoted above each panel; f) the adjusted net heat flux field for F3c, in this case the global mean net heat flux is denoted above the panel.

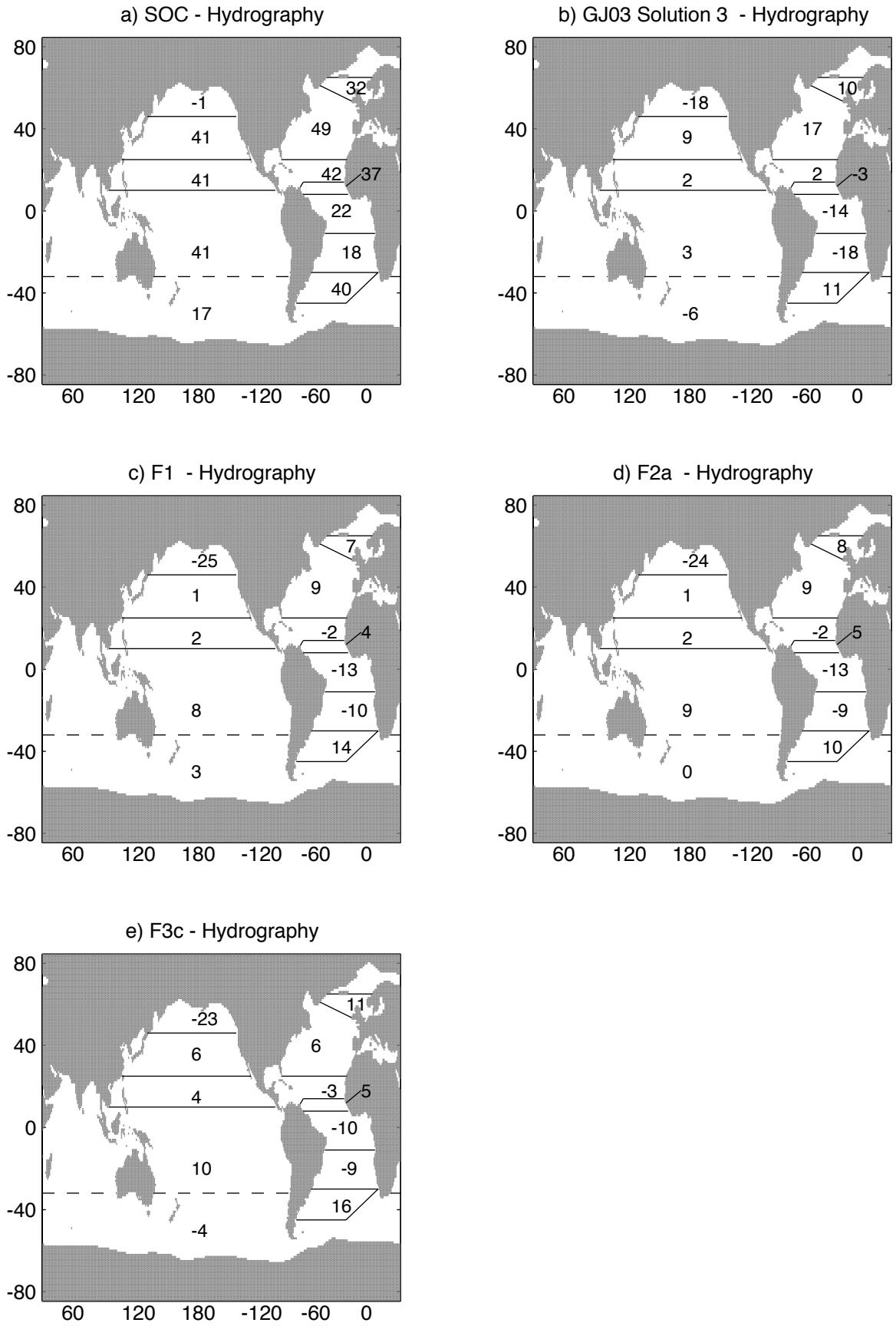

Fig. 17) The difference (climatology - hydrography) between area-averaged net heat flux values from the SOC climatology and hydrography for a) the original SOC climatology, b) the SOC climatology adjusted according to GJ03 Solution 3, c) the SOC climatology adjusted according to F1, d) the SOC climatology adjusted according to F2a and e) the SOC climatology adjusted according to F3c. Units are Wm^{-2}.

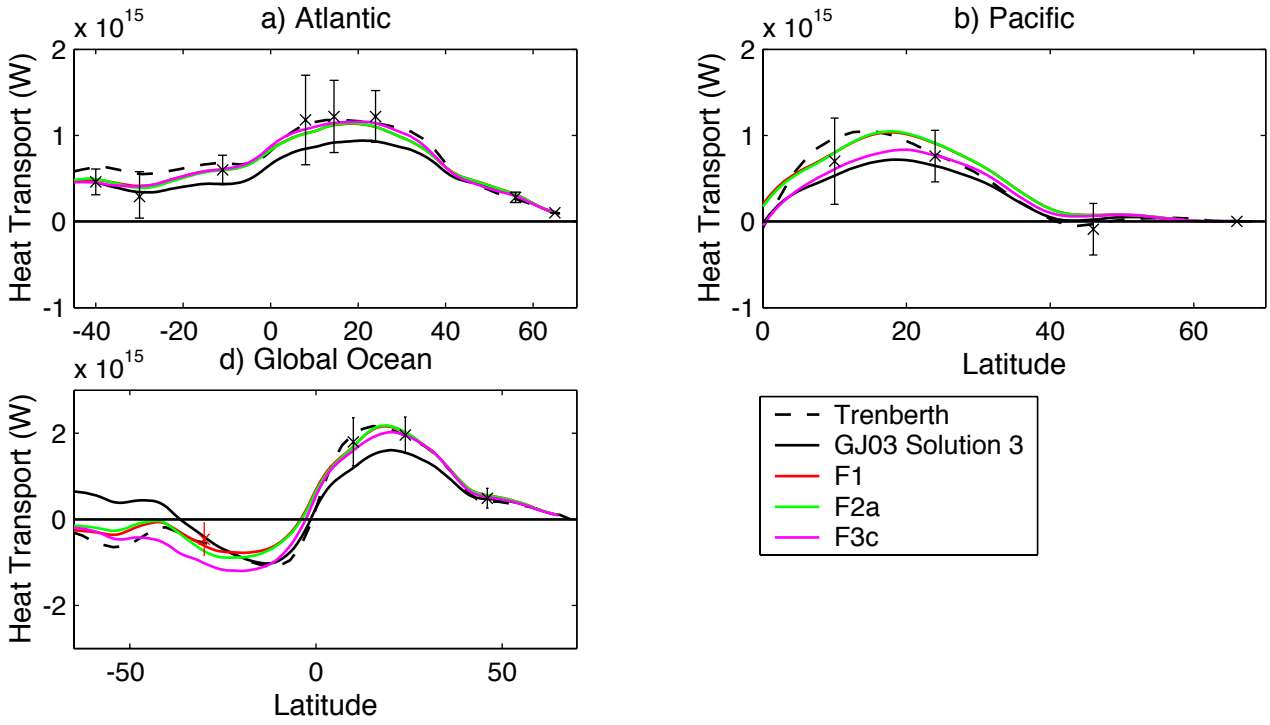

Fig. 18) Ocean heat transport as calculated from various climatologies: SOC GJ03 Solution 3 (solid black line), Trenberth residual (dashed black line), F1 (solid red line), F2a (solid green line) and F3c (solid magenta line), for a) the Atlantic Ocean, b) the Pacific Ocean and c) the Global Ocean. The black crosses indicate hydrographic estimates of the heat transport that were used in the inverse analysis, the red cross is a more recent estimate based on Wijffels et al. (2001).

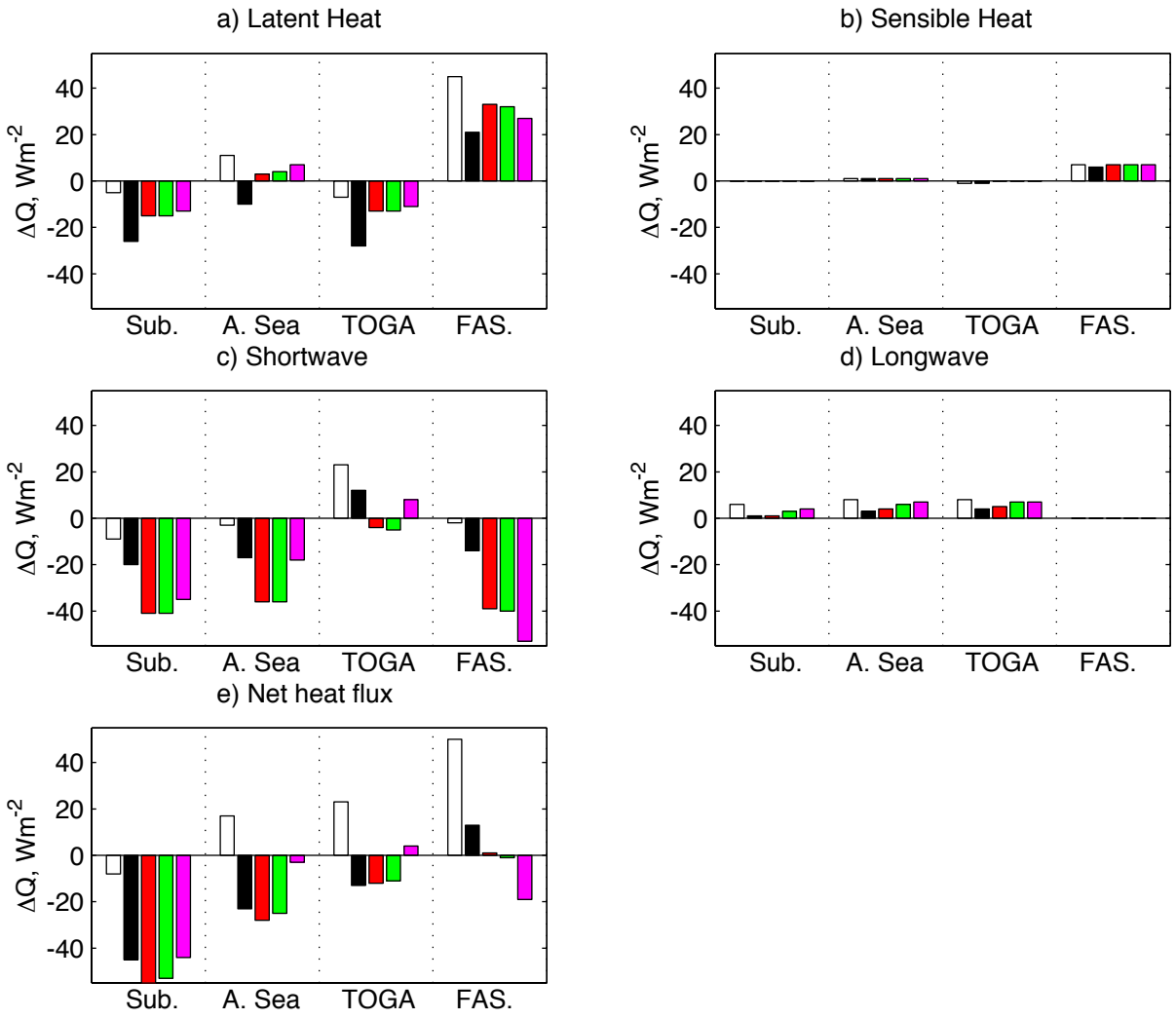

Fig. 19) Summary plot showing the difference (Δ Q) between SOC estimates and WHOI research buoy measurements of heat flux components and the net heat flux for various buoy deployments. White bars: differences between the original SOC climatology and the buoys. Black bars: differences between GJ03 Solution 3 and the buoys. Red bars: differences between F1 and the buoys. Green bars: differences between F2a and the buoys. Magenta bars: differences between F3c and the buoys. The abbreviations refer to the different buoys considered as follows: Sub. refers to the mean of the Subduction Buoy array; A. Sea to the Arabian Sea buoy; TOGA to the TOGA-COARE buoy; and FAS. to the mean of the FASINEX buoy array. Note that buoy measurements of the longwave were not available for FASINEX and that in this case the net heat flux differences are an approximation based on the sum of the latent, sensible and shortwave fluxes.